

Astrocytic adenosine receptor A_{2A} and G_s-coupled signaling regulate memory

Anna G Orr^{1,2}, Edward C Hsiao^{3,4}, Max M Wang¹, Kaithlyn Ho¹, Daniel H Kim¹, Xin Wang¹, Weikun Guo¹, Jing Kang¹, Gui-Qiu Yu¹, Anthony Adame^{5,6}, Nino Devidze¹, Dena B Dubal^{1,2}, Eliezer Masliah^{5,6}, Bruce R Conklin^{3,7} & Lennart Mucke^{1,2}

Astrocytes express a variety of G protein-coupled receptors and might influence cognitive functions, such as learning and memory. However, the roles of astrocytic G_s-coupled receptors in cognitive function are not known. We found that humans with Alzheimer's disease (AD) had increased levels of the G_s-coupled adenosine receptor A_{2A} in astrocytes. Conditional genetic removal of these receptors enhanced long-term memory in young and aging mice and increased the levels of *Arc* (also known as *Arg3.1*), an immediate-early gene that is required for long-term memory. Chemogenetic activation of astrocytic G_s-coupled signaling reduced long-term memory in mice without affecting learning. Like humans with AD, aging mice expressing human amyloid precursor protein (hAPP) showed increased levels of astrocytic A_{2A} receptors. Conditional genetic removal of these receptors enhanced memory in aging hAPP mice. Together, these findings establish a regulatory role for astrocytic G_s-coupled receptors in memory and suggest that AD-linked increases in astrocytic A_{2A} receptor levels contribute to memory loss.

Adenosine is a potent neuromodulator derived from ATP and other adenine nucleotides¹. Adenosine and ATP are released in the brain by diverse cell types under normal and pathological conditions². The adenosine receptors A₁ and A₃ are coupled to G_i, whereas the adenosine receptors A_{2A} and A_{2B} are coupled to G_s and trigger intracellular cyclic AMP (cAMP)-mediated signaling. A_{2A} receptors are highly expressed in the brain and have been implicated in diverse neuropathologies, including Parkinson's disease (PD), ischemic brain injury and traumatic brain injury^{3,4}. These broad effects have been suggested to be at least partly a result of A_{2A} receptors found in glial cells and their roles in neuroinflammatory and neuromodulatory processes⁴. Indeed, the A_{2A} receptor regulates microglial and astrocytic functions and its levels are increased in reactive microglia under certain conditions^{5–7}.

A_{2A} receptors have also been implicated in AD^{8,9}, a neurodegenerative disorder that causes memory loss, synaptic and network dysfunctions, and alterations in glial cells^{10,11}. However, the roles of glial A_{2A} receptors in AD-related cognitive deficits have not been examined. We found that astrocytes, but not microglia, had increased levels of A_{2A} receptor expression in humans with AD. Because the roles of astrocytic A_{2A} receptors and G_s-coupled signaling in cognitive function and neurodegenerative conditions are not known, we investigated the effects of astrocytic A_{2A} receptors and G_s-coupled signaling on learning and memory using conditional genetic ablation of *Adora2a* (the gene encoding A_{2A} receptors) and chemogenetic stimulation of G_s-coupled signaling in astrocytes (**Supplementary Fig. 1a–c**).

We also examined the link between AD and astrocytic A_{2A} receptors using relevant transgenic mouse models.

RESULTS

Astrocytic A_{2A} receptors are increased in humans with AD

We found increased levels of A_{2A} receptor protein in the hippocampal formation, but not frontal cortex, of humans with AD as compared with aged controls (**Fig. 1a** and **Supplementary Table 1**). Although increased A_{2A} receptor ligand binding has been reported in the frontal cortex of AD patients, the levels of A_{2A} receptor protein and mRNA in this region were not altered⁸, consistent with our findings. ADORA2A mRNA levels in the dentate gyrus of AD patients were also increased and strongly correlated with AD pathology, as classified by the Braak score¹², a measure of neurofibrillary tangles and disease progression (Spearman rank correlation, $R = 0.76$, $P = 0.0063$, $n = 11$ cases; **Fig. 1b,c**). ADORA2A mRNA levels also correlated with the levels of mRNA encoding glial fibrillary acidic protein (GFAP), a marker of astrogliosis (Spearman rank correlation, $R = 0.57$, $P = 0.027$, $n = 15$ cases; **Fig. 1d**).

A_{2A} receptors are expressed by various cell types in the brain, including neurons, microglia and astrocytes^{1,3,6}. We examined whether A_{2A} receptors are expressed by glial cells in the human brain and whether the levels of these receptors are altered in AD. Aging humans without dementia had low levels of A_{2A} receptor expression in astrocytes (**Fig. 1e,f** and **Supplementary Table 1**), consistent with previous reports in primates³. However, in two different cohorts of AD

¹Gladstone Institute of Neurological Disease, San Francisco, California, USA. ²Department of Neurology, University of California, San Francisco, California, USA.

³Gladstone Institute of Cardiovascular Disease, San Francisco, California, USA. ⁴Division of Endocrinology and Metabolism, Department of Medicine, and the Institute for Human Genetics, University of California, San Francisco, California, USA. ⁵Department of Neuroscience, University of California, San Diego, La Jolla, California, USA. ⁶Department of Pathology, University of California, San Diego, La Jolla, California, USA. ⁷Department of Cellular and Molecular Pharmacology, University of California, San Francisco, California, USA. Correspondence should be addressed to A.G.O. (anna.orr@gladstone.ucsf.edu) or L.M. (lmucke@gladstone.ucsf.edu).

Received 10 October 2014; accepted 15 December 2014; published online 26 January 2015; doi:10.1038/nn.3930

patients, we found marked increases in astrocytic, but not microglial, A_{2A} receptor expression in the hippocampal formation, as determined by co-immunolabeling for A_{2A} and the astrocyte marker aldehyde dehydrogenase 1 family member L1 (Aldh1L1)¹³, or the microglial marker ionized calcium-binding adaptor molecule 1 (Iba1; Fig. 1e–g and Supplementary Fig. 1d).

We next examined whether A_{2A} receptors expressed by astrocytes are coupled to G_s, as they are in other cell types¹. Although A_{2A} receptors were expressed by astrocytes in brains of adult humans (this study), other primates and rodents^{3,14}, A_{2A} receptor expression was not detectable in cultured postnatal mouse astrocytes by western blotting or agonist-induced cAMP measurements (Supplementary Fig. 2a,b), consistent with previous studies⁵. However, in cultured mouse astrocytes transduced with a lentivirus encoding the mouse A_{2A} receptor, adenosine and the A_{2A}-selective agonist CGS-21680 increased the levels of intracellular cAMP and phosphorylated ERK and CREB, but did not affect intracellular calcium levels (Supplementary Fig. 2a–e),

Figure 1 Astrocytic A_{2A} receptor expression is increased in humans with AD. (a) Levels of A_{2A} receptor protein in hippocampi (HP) and frontal cortices (FC) of human control (Con) and AD cases as determined by western blotting. Ratios of A_{2A}/actin were normalized to the average ratio in control samples. Student's *t* test with Welch's correction (Con versus AD): P = 0.001 (HP); P = 0.70 (FC). n = 5 (Con HP), 17 (AD HP), 5 (Con FC) and 16 (AD FC) cases per group. (b) Levels of ADORA2A and GFAP mRNA in the dentate gyrus from Con and AD cases as determined by quantitative reverse transcription PCR (qRT-PCR). GAPDH mRNA served as a loading control. Student's *t* test with Welch's correction (Con versus AD): P = 0.0008 (ADORA2A); P < 0.0001 (GFAP). n = 3 (Con ADORA2A), 15 (AD ADORA2A), 3 (Con GFAP) and 16 (AD GFAP) cases per group. (c) Levels of ADORA2A mRNA in the dentate gyrus of humans with AD ranging from mild to severe on the basis of pathological analysis and Braak scoring¹². ADORA2A/GAPDH ratios were plotted as a function of Braak score. Spearman rank correlation, R = 0.76, P = 0.0063, n = 11 cases. The red line indicates the linear regression curve and the dotted lines show the 95% confidence intervals. (d) Levels of ADORA2A mRNA in the dentate gyrus of humans with AD plotted as a function of GFAP mRNA levels. Spearman rank correlation, R = 0.57, P = 0.027, n = 15 cases. GAPDH mRNA served as a loading control. (e,f) Representative photomicrographs of A_{2A} receptor immunoreactivity in hippocampal sections from two independent cohorts of human cases with the indicated Braak stages. Severity of cognitive impairment is indicated by Mini Mental State Examination (MMSE) or Blessed Dementia Scale (BDS) scores. Insets (i–iv) show magnified views of the boxed regions. (g) Representative photomicrographs of a hippocampal section from an AD case co-immunostained for the A_{2A} receptor (green) and the astrocyte marker Aldh1L1 (red). Cell nuclei were labeled with DAPI (blue). The overlay shows colocalization of A_{2A} and Aldh1L1 immunoreactivities. Scale bars represent 100 μ m (e–g, main panels) and 25 μ m (bottom insets in g). n = 10 Con and 19 AD cases. Insets (i–vi) show magnified views of the boxed regions. ***P < 0.001 (Student's *t* test with Welch's correction). Data are presented as mean \pm s.e.m.

confirming that A_{2A} receptor activation induces G_s-coupled, but not G_q-coupled, signaling in astrocytes.

Mice with conditional ablation of astrocytic A_{2A} receptors

Because it is unknown whether astrocytic A_{2A} receptors have any role in cognition, we next examined whether conditional genetic ablation of these receptors affects learning and memory in mice. Transgenic mice lacking A_{2A} receptors in astrocytes were generated using a GFAP promoter-driven Cre recombinase/loxP system. Specifically, we bred mice in which the *Adora2a* gene was flanked by two loxP sequences (loxP-*Adora2a*)¹⁵ with mice that express Cre recombinase under control of the GFAP promoter¹⁶, resulting in transgenic offspring in which no (A_{2A}-cWT), one (A_{2A}-cHET) or both (A_{2A}-cKO) *Adora2a* genes were deleted mainly during late embryonic development in GFAP-expressing cells (Supplementary Fig. 1a)¹⁷. A_{2A}-cWT mice expressed Cre, but did not carry loxP-*Adora2a* alleles, whereas A_{2A}-cHET and A_{2A}-cKO mice expressed Cre and carried one or two loxP-*Adora2a*

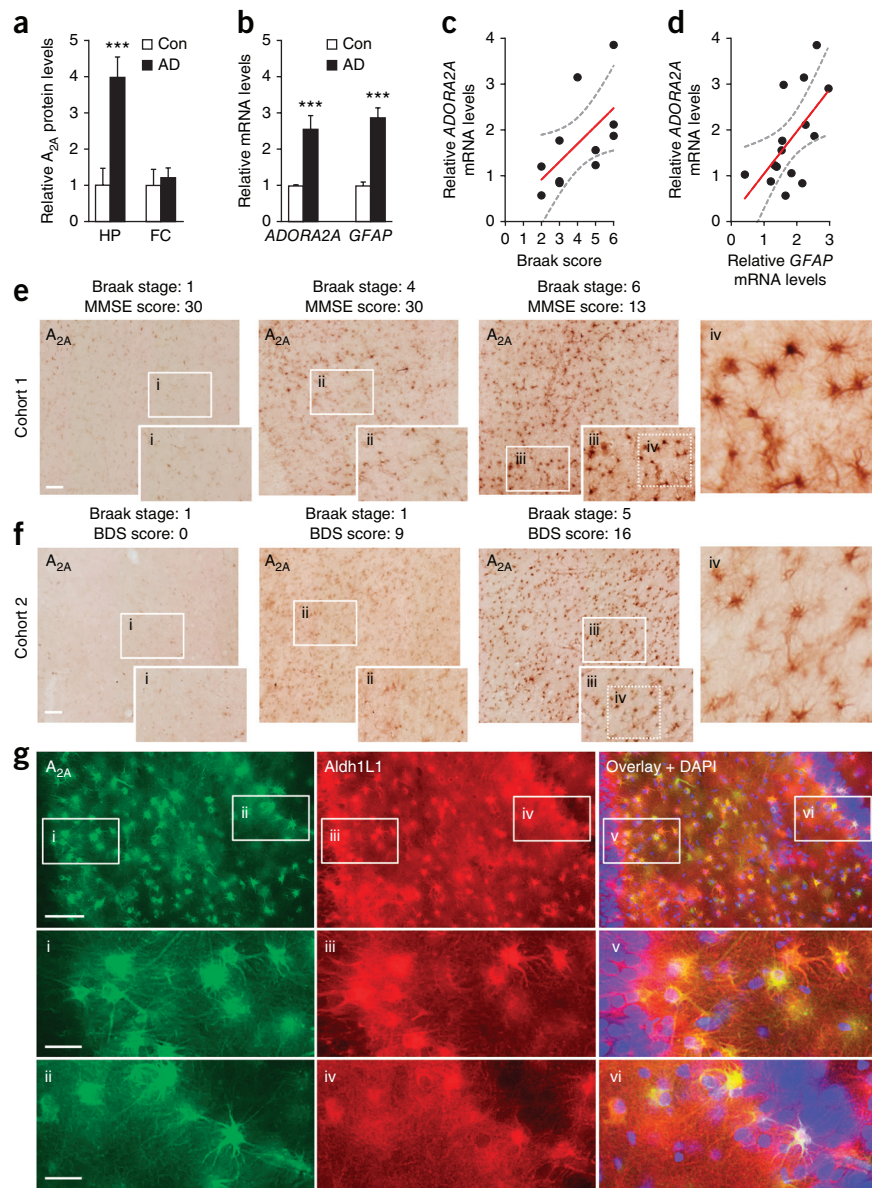


Figure 2 Conditional ablation of A_{2A} receptors in astrocytes enhances memory in mice.

(a,b) GFAP-Cre/loxP-Adora2a mice were tested in the Morris water maze at 2–4 months of age. (a) Distance traveled to reach the platform during hidden platform training (two trials per session, two sessions per day for 4 d). Repeated measures two-way ANOVA: $F(14, 308) = 0.34, P = 0.99$ for interaction effect, $F(2, 44) = 1.34, P = 0.27$ for genotype effect. $n = 12$ A_{2A}-cWT, 18 A_{2A}-cHET and 17 A_{2A}-cKO mice. (b) Probe trial conducted 6 d after training. Left, durations in target and non-target (other) quadrants. One-way ANOVA: $F(2, 42) = 3.09, P = 0.056$; one-sample t test versus chance duration of 15 s with FDR correction for multiple comparisons (target versus chance): $P = 0.36$ (cWT), $P = 0.018$ (cHET), $P = 0.0075$ (cKO). $n = 11$ cWT, 18 cHET and 16 cKO mice. # $P < 0.05$ versus cWT (Dunnett's test); * $P < 0.05$, ** $P < 0.01$ (one-sample t test).

Right, crossings of target and non-target (other) platform locations. Two-way ANOVA: $F(2, 85) = 3.66, P = 0.03$ for interaction effect; $F(2, 85) = 2.45, P = 0.09$ for genotype effect. Student's t test with Welch's correction (target versus other of matching genotype): $P = 0.35$ (cWT), $P = 0.85$ (cHET), $P = 0.0003$ (cKO). *** $P < 0.001$ (Student's t test with Welch's correction).

(c–f) GFAP-Cre/loxP-Adora2a mice were tested in the open field in 5-min trials (1–2 trials per day) for 3 d

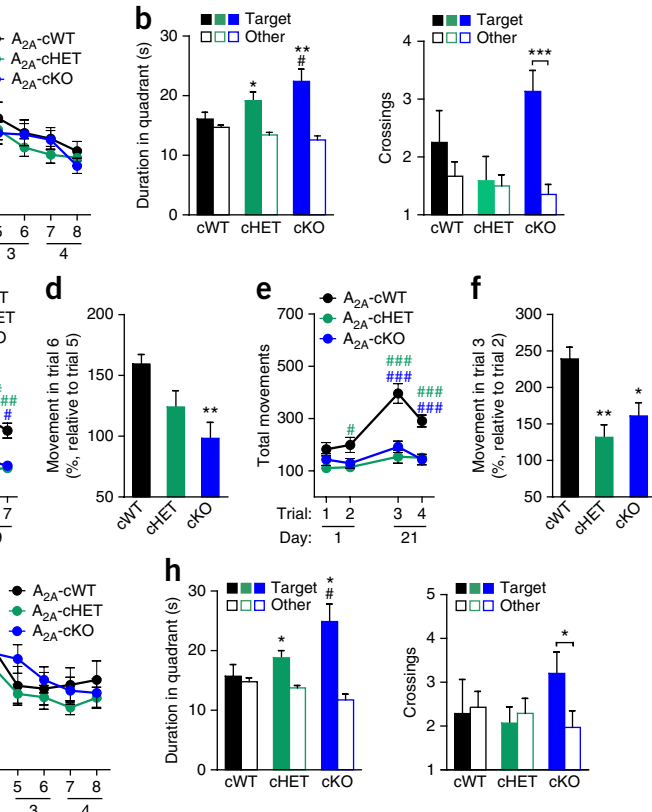
and tested in the same arena 6 d later (day 9). (c) Repeated measures two-way ANOVA: $F(12, 264) = 1.14, P = 0.33$ for interaction effect, $F(2, 44) = 14.99, P < 0.0001$ for genotype effect. $n = 12$ A_{2A}-cWT, 18 A_{2A}-cHET and 17 A_{2A}-cKO mice. # $P < 0.05$, ## $P < 0.01$, ### $P < 0.001$ versus A_{2A}-cWT (Bonferroni). Green hash tags indicate differences between A_{2A}-cWT and A_{2A}-cHET groups, and blue hash tags indicate differences between A_{2A}-cWT and A_{2A}-cKO groups. (d) Extent of dishabituation on day 9 after mice had not been tested in the same open field for 6 d (test trial 6 relative to trial 5). One-way ANOVA: $F(2, 41) = 4.79, P = 0.014$. $n = 11$ A_{2A}-cWT, 17 A_{2A}-cHET and 17 A_{2A}-cKO mice. ** $P < 0.01$ versus cWT (Dunnett's test).

(e,f) Mice were re-habituated to the open field in two 5-min trials in 1 d and tested 20 d later (day 21). (e) Repeated measures two-way ANOVA: $F(6, 132) = 4.38, P = 0.0005$ for interaction effect, $F(2, 44) = 25.61, P < 0.0001$ for genotype effect. $n = 12$ A_{2A}-cWT, 18 A_{2A}-cHET and 17 A_{2A}-cKO mice. # $P < 0.05$, ## $P < 0.001$ versus A_{2A}-cWT (Bonferroni). (f) Extent of dishabituation on day 21 (test trial 3 relative to trial 2). One-way ANOVA: $F(2, 42) = 8.27, P = 0.0009$. $n = 11$ cWT, 17 cHET and 17 cKO mice. * $P < 0.05$, ** $P < 0.01$ versus cWT (Dunnett's test).

(g,h) GFAP-Cre/loxP-Adora2a mice were tested in the Morris water maze at 15–17 months of age. (g) Distance traveled to reach the platform during hidden platform training (two trials per session, two sessions per day for 4 d). Repeated measures two-way ANOVA: $F(14, 217) = 0.60, P = 0.86$ for interaction effect, $F(2, 31) = 1.80, P = 0.18$ for genotype effect. $n = 7$ A_{2A}-cWT, 15 A_{2A}-cHET and 11 A_{2A}-cKO mice. (h) Probe trial conducted 6 d after training. Left, durations in target and non-target (other) quadrants. One-way ANOVA: $F(2, 30) = 4.36, P = 0.022$; one-sample t test versus chance duration of 15 s with FDR correction for multiple comparisons (target versus chance): $P = 0.73$ (cWT), $P = 0.011$ (cHET), $P = 0.011$ (cKO). $n = 7$ A_{2A}-cWT, 15 A_{2A}-cHET and 11 A_{2A}-cKO mice. * $P < 0.05$ (one-sample t test). # $P < 0.05$ versus cWT (Dunnett's test). Right, crossings of target and non-target (other) platform locations. Two-way ANOVA: $F(2, 59) = 1.75, P = 0.18$ for interaction effect, $F(2, 59) = 0.49, P = 0.61$ for genotype effect. Student's t test with Welch's correction (target versus other of matching genotype): $P = 0.87$ (cWT), $P = 0.66$ (cHET), $P = 0.037$ (cKO). * $P < 0.05$ (Student's t test with Welch's correction). Data are presented as mean \pm s.e.m.

alleles, respectively. GFAP is expressed mostly in astrocytes, and previous studies have shown that Cre expression and Cre-mediated gene ablation are found primarily in astrocytes in this transgenic system^{7,18–20}. However, the *Gfap* promoter shows some activity in neural progenitors²¹, which could result in Cre-mediated A_{2A} receptor ablation in some neuronal populations. Thus, we first tested whether neuronal A_{2A} receptor expression was preserved in these mice, as reported previously²².

The A_{2A} receptor is highly expressed in striatal neurons¹ and moderately expressed in hippocampal neurons²³. Using a well-characterized monoclonal antibody for the A_{2A} receptor^{3,15}, we found comparable levels of neuronal A_{2A} receptor immunoreactivity in the striatum of A_{2A}-cWT, A_{2A}-cHET and A_{2A}-cKO mice (Supplementary Fig. 3a), indicating that A_{2A} receptors were not ablated in striatal neurons. Minimal immunolabeling was detected in global homozygous A_{2A} receptor knockout mice (A_{2A}-gKO, also known as *Adora2a*^{-/-};



Supplementary Fig. 3a), confirming antibody specificity. Neuronal A_{2A} receptor expression was also preserved in the CA1 region of the hippocampal formation (Supplementary Fig. 3b). In contrast, astrocytic A_{2A} receptors were ablated in both A_{2A}-cKO and A_{2A}-gKO mice (Supplementary Fig. 3c).

Ablation of astrocytic A_{2A} receptors enhances memory

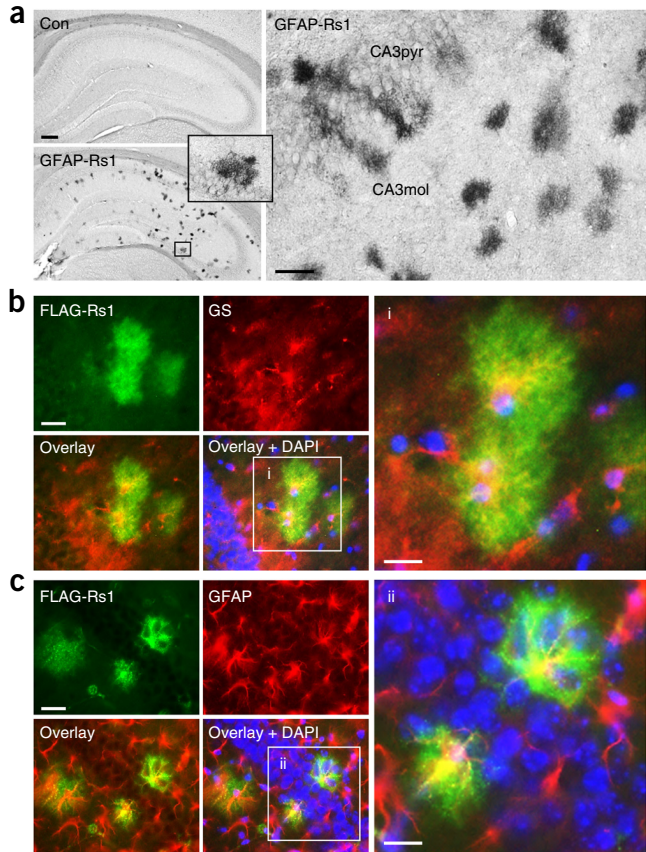
We next assessed learning and memory in 2–4-month-old A_{2A}-cWT, A_{2A}-cHET and A_{2A}-cKO mice in the Morris water maze. In this test, mice learn to locate a hidden platform using spatial cues outside of the maze. Specifically, the mice underwent 4 d of hidden platform training (two sessions per day and two trials per session). After completion of training, a probe trial was performed in which the platform was removed and putative indices of spatial memory were measured. Ablation of astrocytic A_{2A} receptors did not affect learning during hidden platform training (Fig. 2a). However, in comparison

Figure 3 Generation of GFAP-Rs1 transgenic mice. **(a)** Representative photomicrographs of FLAG-immunostained brain sections of 2–11-month-old GFAP-tTA singly transgenic control mice (Con) and GFAP-Rs1 double transgenic mice. Inset, magnified view of the boxed region. Scale bars represent 200 μ m (left) and 50 μ m (right). CA3pyr, Cornu Ammonis 3 (CA3) pyramidal cell layer; CA3mol, CA3 molecular layer. $n = 9$ Con and 15 GFAP-Rs1 mice. **(b,c)** Representative photomicrographs of the hippocampal formation of GFAP-Rs1 mice immunostained for FLAG-Rs1 and astrocyte markers glutamine synthetase (GS, **b**) or GFAP (**c**). Cell nuclei were labeled with DAPI (blue). $n = 6$ Con and 8 GFAP-Rs1 mice. Main scale bars represent 50 μ m. Insets (i,ii) show magnified views of the boxed regions. Inset scale bars represent 25 μ m.

with A_{2A}-cWT mice, A_{2A}-cHET and A_{2A}-cKO mice showed enhanced memory in a probe trial conducted 6 d after training (Fig. 2b). Specifically, A_{2A}-cHET and A_{2A}-cKO mice showed a persistent memory for the target quadrant. A_{2A}-cKO mice also remembered the platform location (Fig. 2b), suggesting that the ablation of astrocytic A_{2A} receptors enhances spatial memory. Swim speeds during the probe trial were similar among the groups (Supplementary Fig. 4a).

To confirm these results in another behavioral test of learning and memory, we next examined the effects of astrocytic A_{2A} receptor ablation on contextual memory by measuring the levels of habituation to a novel environment²⁴. The same cohort of transgenic mice that was tested in the Morris water maze was habituated for 3 d to an open field chamber and tested in the same chamber 6 d later (day 9). A_{2A}-cHET and A_{2A}-cKO mice habituated at the same rate as A_{2A}-cWT mice, suggesting similar rates of contextual learning (Fig. 2c). However, A_{2A}-cHET and A_{2A}-cKO mice showed lower levels of activity during habituation than A_{2A}-cWT mice (Fig. 2c), as observed with global ablation of the A_{2A} receptor²⁵, but not with ablation restricted to forebrain neurons²⁶. On day 9, A_{2A}-cWT mice showed marked dishabituation, consistent with contextual memory loss, whereas A_{2A}-cHET and A_{2A}-cKO mice showed lower or no dishabituation, respectively (Fig. 2c,d). We also tested whether the contextual memory in A_{2A}-cHET and A_{2A}-cKO mice would persist despite a longer delay. Mice were re-habituated to the same open field chamber for 1 d and tested on day 21. A_{2A}-cWT mice showed robust dishabituation on day 21 (Fig. 2e,f), suggesting a loss of contextual memory. In contrast, both A_{2A}-cHET and A_{2A}-cKO mice showed lower levels of dishabituation (Fig. 2e,f), suggesting that reduction or ablation of astrocytic A_{2A} receptors prolongs the retention of contextual memory. Anxiety-related behavior in the open field, as measured by the amount of time spent in the center of the field, did not differ between genotypes (Supplementary Fig. 4c,d).

Aging animals show astrocytic hypertrophy²⁷ and a decline in memory²⁸. We tested whether ablation of astrocytic A_{2A} receptors also enhances spatial memory in aging mice. At 15–17 months of age, the same cohort of A_{2A}-cWT, A_{2A}-cHET and A_{2A}-cKO mice was retested in the Morris water maze using a different set of cues and a different platform location. Consistent with the normal learning in 2–4-month-old A_{2A}-cHET and A_{2A}-cKO mice (Fig. 2a), 15–17-month-old A_{2A}-cHET and A_{2A}-cKO mice learned the new platform location as well as age-matched A_{2A}-cWT mice (Fig. 2g). As observed in young mice, aging A_{2A}-cHET and A_{2A}-cKO mice showed enhanced memory 6 d after training. In contrast with A_{2A}-cWT mice, A_{2A}-cHET and A_{2A}-cKO mice showed a persistent memory for the target quadrant, and A_{2A}-cKO mice also remembered the platform location (Fig. 2h). Swim speeds during the probe trial were similar among the groups (Supplementary Fig. 4b). These results suggest that the effects of astrocytic A_{2A} receptors on memory persist with age.



We next examined whether the conditional knockout mice showed changes in signaling factors known to regulate long-term memory. To begin to address this question, we focused on the immediate-early gene *Arc* (also known as *Arg3.1*), which is involved in long-term memory, but not learning or short-term memory²⁹. We found that mice with conditional ablation of astrocytic A_{2A} receptors had increased levels of Arc expression in the dentate gyrus and cortex (Supplementary Fig. 5), indicating that memory modulation by astrocytic A_{2A} receptors is associated with changes in Arc levels.

Chemogenetic control of astrocytic G_s-coupled signaling

Our findings in conditional knockout mice suggest that A_{2A} receptors were ablated primarily in astrocytes. However, we cannot completely exclude the possibility that A_{2A} receptor expression was reduced in some neuronal populations. Furthermore, genetic ablation of *Adora2a* might affect early brain development or induce compensatory changes that could be independent of A_{2A} receptor activity *per se*. To overcome these potential limitations, we used an inducible tet-off system and recently developed chemogenetic tools to test the effects of acutely modulating astrocytic G_s-coupled receptor activity in adult behaving mice. Whereas optogenetics introduces light-sensitive ion channels or other proteins into specific cell populations, chemogenetics uses receptors that are activated solely by synthetic ligands. Chemogenetics enables selective and noninvasive stimulation of G protein-coupled receptors in specific cell populations in awake, behaving animals³⁰. We used this approach to further examine the roles of astrocytic G_s-coupled receptors in cognitive functions and behavior.

To manipulate astrocytic G_s-coupled receptor signaling in adulthood in a cell- and receptor-selective manner, we generated inducible GFAP-tTA/TetO-Rs1 doubly transgenic mice (GFAP-Rs1 mice) in which astrocytic expression of a modified G_s-coupled receptor

(Rs1)³¹ is regulated by a tTA/TetO system under the control of the human GFAP promoter (**Supplementary Fig. 1b,c**). Rs1 is the human G_s-coupled 5-HT_{4b} serotonin receptor containing a single D100A mutation that renders it insensitive to serotonin, but highly sensitive to synthetic ligands that minimally activate endogenous receptors³¹. As expected, Rs1 expression was suppressed by doxycycline (DOX) in GFAP-Rs1 mice and was absent in *GFAP-tTA* and *TetO-Rs1* singly transgenic mice (**Fig. 3a** and **Supplementary Fig. 6a,b**). We prevented Rs1 expression during development by maintaining all

breeding pairs and offspring used in subsequent experiments on a DOX-supplemented diet until weaning at 3 weeks of age, after which DOX was removed to initiate Rs1 expression. By 2 months of age, Rs1 expression was detected in the hippocampal formation and thalamus (**Fig. 3a** and **Supplementary Fig. 6a-d**), but was minimal in the cortex (data not shown). Rs1 expression was selective for astrocytes, which appeared to be highly branched and wrapped around neuronal cell bodies (**Fig. 3b-c**), as is typical for this cell type³². The proportion of astrocytes immunoreactive for Rs1 was relatively low, possibly as

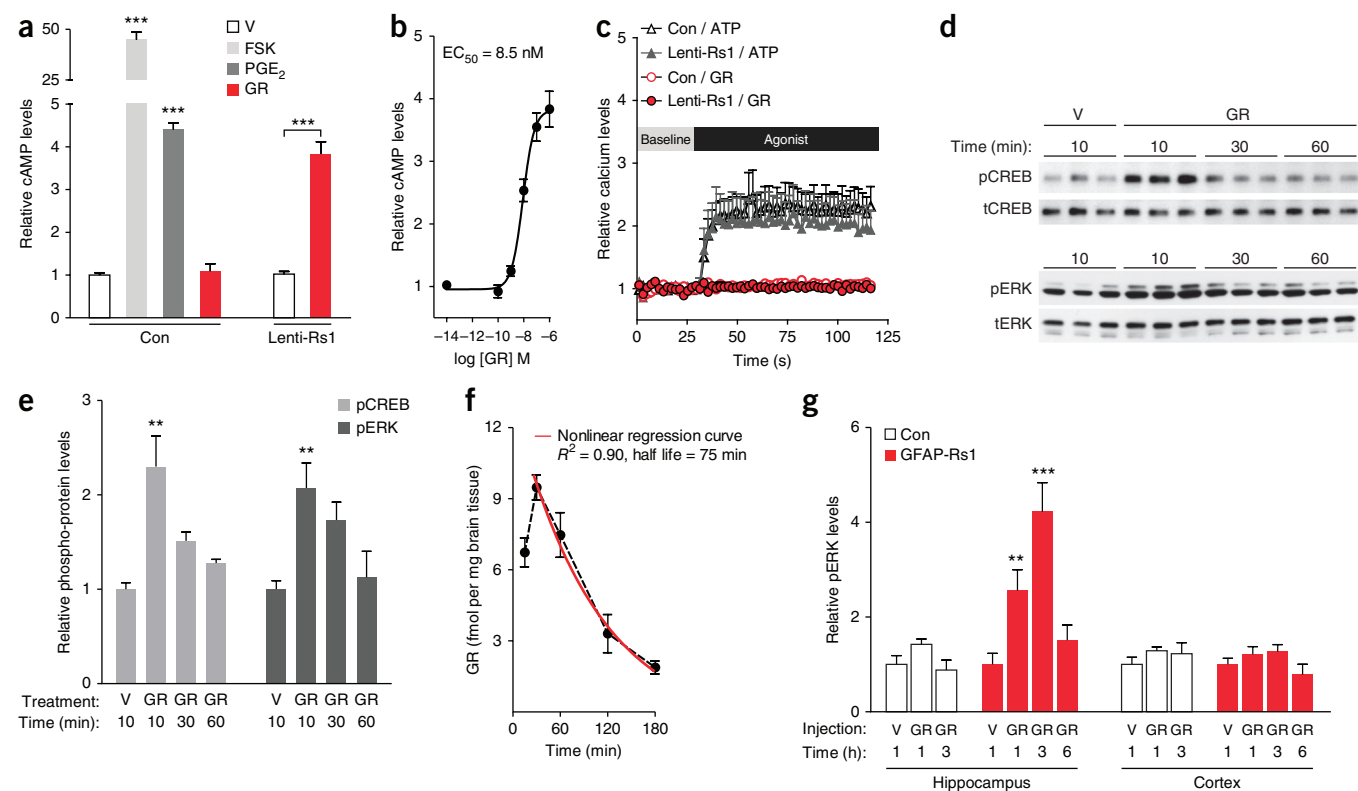
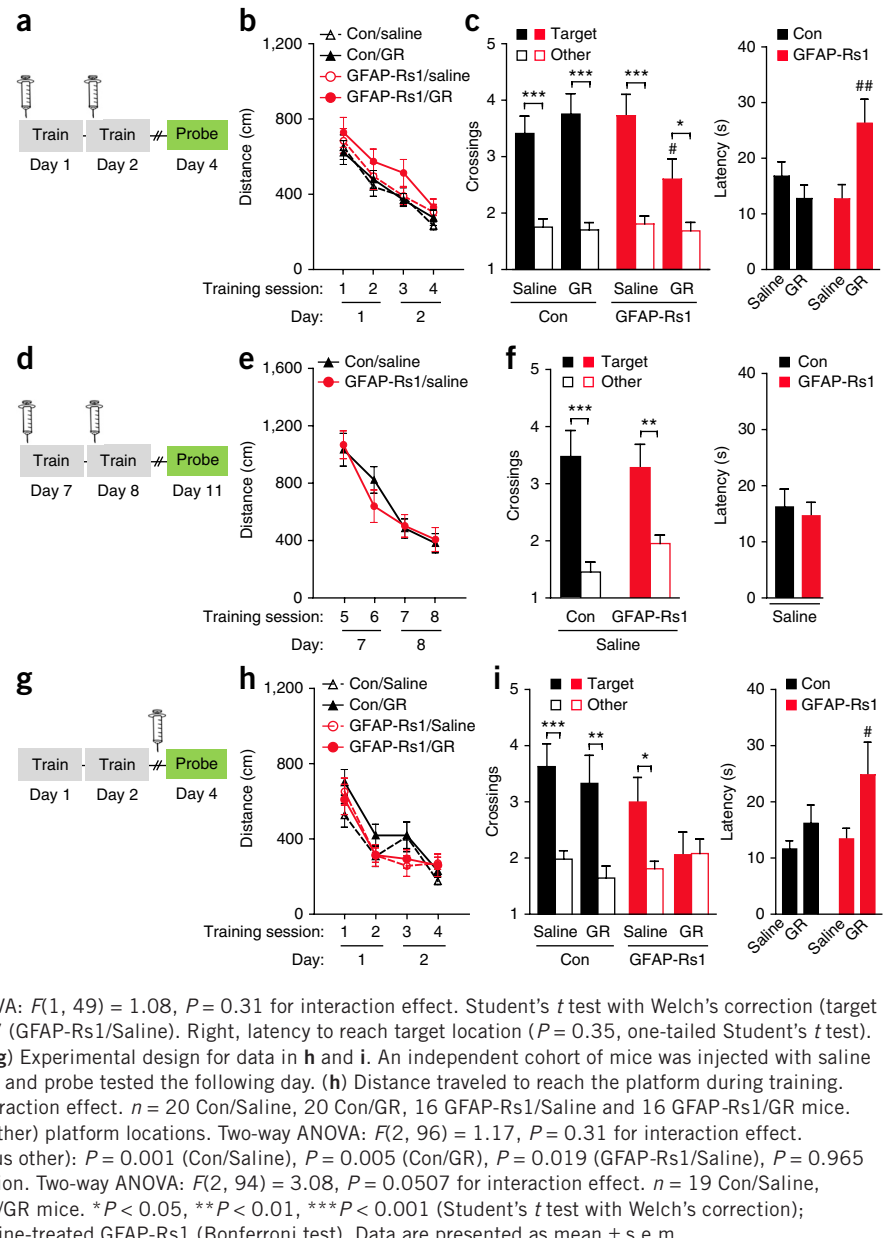


Figure 4 Rs1 ligand increases G_s-coupled signaling in Rs1-expressing astrocytes. (a) Relative cAMP levels in primary astrocyte cultures established from non-transgenic mice and transduced (Lenti-Rs1) or not (Con) with a lentivirus encoding Rs1. Following 15-min treatment with vehicle (V) or the Rs1 ligand GR-125487 (GR, 1 μM), cultures were analyzed for intracellular cAMP levels. Forskolin (FSK, 30 μM) and prostaglandin E₂ (PGE₂, 40 μM) served as positive controls. cAMP levels were normalized to the average levels in vehicle-treated cells in each transduction condition. Two-way ANOVA: $F(1, 35) = 81.75, P < 0.0001$ for interaction effect. One-way ANOVA: $F(3, 38) = 729.7, P < 0.0001$. $n = 15$ Con/V, 3 Con/FSK, 16 Con/PGE₂, 8 Con/GR, 8 Lenti-Rs1/V and 8 Lenti-Rs1/GR wells from three independent experiments. *** $P < 0.001$ versus leftmost bar (Dunnett's test) or as indicated by bracket (Bonferroni test). (b) Dose-response curve for relative cAMP levels after GR treatment in Lenti-Rs1-transduced astrocytes. $n = 8$ (10^{-14} M), 7 (10^{-10} M), 6 (10^{-9} M), 6 (10^{-8} M), 9 (10^{-7} M) and 8 (10^{-6} M) wells from 2–3 independent experiments. $R^2 = 0.866$. (c) Calcium levels in primary astrocyte cultures transduced as in a. Cells were treated with GR (10 μM) or ATP (100 μM) and assayed for intracellular calcium levels with calcium-5, a calcium-sensitive fluorescent dye. Fluorescence intensities were normalized to the average baseline intensity in each well. The maximum intensities per well were compared between groups. Two-way ANOVA: $F(1, 20) = 0.14, P = 0.72$ for interaction effect, $F(1, 20) = 14.57, P = 0.0011$ for agonist effect, $F(1, 20) = 0.16, P = 0.69$ for Lenti-Rs1 effect. $n = 6$ wells per condition from two independent experiments. (d,e) Proteins regulated by G_s-coupled signaling were quantified in Lenti-Rs1-transduced astrocytes by western blot analysis after treating cultures with vehicle or GR (1 μM) for the indicated durations. Representative cropped western blots (d) and densitometric quantification of western blot signals (e). Blots were probed for phosphorylated (p) and total (t) CREB and ERK. Ratios of phosphorylated/total protein were normalized to the average ratio in vehicle-treated cells. $n = 5$ pCREB/V-10, 7 pCREB/GR-10, 6 pCREB/GR-30, 3 pCREB/GR-60, 6 pERK/V-10, 7 pERK/GR-10, 6 pERK/GR-30 and 3 pERK/GR-60 wells from two independent experiments. One-way ANOVA: $F(3, 17) = 6.61, P = 0.0037$ (pCREB); $F(3, 18) = 5.66, P = 0.0065$ (pERK); ** $P < 0.01$ versus V (Dunnett's test). Full-length blots are presented in **Supplementary Figure 13**. (f) GR concentration in whole hemibrains of 3–4-month-old non-transgenic mice determined by mass spectrometry–high-performance liquid chromatography following a single i.p. injection of GR (1 mg per kg) and transcardial perfusion at the indicated times post-injection. $n = 3$ mice per time point. (g) Hippocampal and cortical pERK levels in 2–4-month-old *GFAP-tTA* (Con) and GFAP-Rs1 mice, as determined by western blot analysis after a single injection of vehicle or GR (3 mg per kg, i.p.). pERK/tERK ratios were normalized to the average ratios in saline-treated mice within each genotype and brain region. Two-way ANOVA: hippocampus, $F(2, 32) = 8.06, P = 0.0015$ for genotype by treatment interaction; cortex, $F(2, 28) = 0.09, P = 0.91$ for genotype by treatment interaction; $n = 5$ HP/Con/V-1h, 10 HP/Con/GR-1h, 4 HP/Con/GR-3h, 5 HP/GFAP-Rs1/V-1h, 10 HP/GFAP-Rs1/GR-1h, 4 HP/GFAP-Rs1/GR-3h, 4 HP/GFAP-Rs1/GR-6h, 5 CTX/Con/V-1h, 10 CTX/Con/GR-1h, 4 CTX/Con/GR-3h, 3 CTX/GFAP-Rs1/V-1h, 8 CTX/GFAP-Rs1/GR-1h, 4 CTX/GFAP-Rs1/GR-3h, and 4 CTX/GFAP-Rs1/GR-6h mice. ** $P < 0.01$, *** $P < 0.001$ versus HP/GFAP-Rs1/V (Bonferroni test). Data are presented as mean ± s.e.m.

Figure 5 Rs1 ligand impairs memory in GFAP-Rs1 mice. *GFAP-tTA* (Con) and GFAP-Rs1 mice were tested in the Morris water maze at 2–11 months of age. (a) Experimental design for data in b and c. On two consecutive days, mice were injected with saline or the Rs1 ligand GR-125487 (GR, 3 mg per kg per d, i.p.) 15 min before hidden platform training. Memory of the platform location was tested in a probe trial (platform removed) 2 d after completing training. (b) Distance traveled to reach the platform during training. Two-way ANOVA: $F(9, 273) = 0.34$, $P = 0.96$ for interaction effect. $n = 27$ Con/Saline, 29 Con/GR, 19 GFAP-Rs1/Saline, and 20 GFAP-Rs1/GR mice. (c) Probe. Left, crossings of target and equivalent non-target (other) locations. Two-way ANOVA: $F(1, 89) = 4.15$, $P = 0.045$ for genotype by treatment interaction. Student's t test with Welch's correction (target versus other): $P < 0.0001$ (Con/Saline), $P < 0.0001$ (Con/GR), $P = 0.0001$ (GFAP-Rs1/Saline), $P = 0.027$ (GFAP-Rs1/GR). *** $P < 0.001$, * $P < 0.05$ (Student's t test with Welch's correction). Right, latency to reach target location. Two-way ANOVA: $F(1, 89) = 8.56$, $P = 0.0044$ for interaction effect. $n = 27$ Con/Saline, 28 Con/GR, 18 GFAP-Rs1/Saline, and 20 GFAP-Rs1/GR mice. (d) Experimental design for data in e and f. Mice previously treated with GR and tested as in a were injected i.p. with saline 15 min before retraining to a new hidden platform location in a new context. Memory was tested in a probe 3 d after completing retraining. (e) Distance traveled to reach the platform during retraining. Two-way ANOVA: $F(3, 75) = 0.72$, $P = 0.54$ for interaction effect. $n = 15$ Con/Saline and 12 GFAP-Rs1/Saline mice. (f) Probe. Left, crossings of target and non-target (other) platform locations. Two-way ANOVA: $F(1, 49) = 1.08$, $P = 0.31$ for interaction effect. Student's t test with Welch's correction (target versus other): $P = 0.0007$ (Con/Saline), $P = 0.0097$ (GFAP-Rs1/Saline). Right, latency to reach target location ($P = 0.35$, one-tailed Student's t test). $n = 15$ Con/Saline and 12 GFAP-Rs1/Saline mice. (g) Experimental design for data in h and i. An independent cohort of mice was injected with saline or GR 1 d after completing hidden platform training and probe tested the following day. (h) Distance traveled to reach the platform during training. Two-way ANOVA: $F(5, 99) = 0.31$, $P = 0.91$ for interaction effect. $n = 20$ Con/Saline, 20 Con/GR, 16 GFAP-Rs1/Saline and 16 GFAP-Rs1/GR mice. (i) Probe. Left, crossings of target and non-target (other) platform locations. Two-way ANOVA: $F(2, 96) = 1.17$, $P = 0.31$ for interaction effect. Student's t test with Welch's correction (target versus other): $P = 0.001$ (Con/Saline), $P = 0.005$ (Con/GR), $P = 0.019$ (GFAP-Rs1/Saline), $P = 0.965$ (GFAP-Rs1/GR). Right, latency to reach target location. Two-way ANOVA: $F(2, 94) = 3.08$, $P = 0.0507$ for interaction effect. $n = 19$ Con/Saline, 18 Con/GR, 16 GFAP-Rs1/Saline and 16 GFAP-Rs1/GR mice. * $P < 0.05$, ** $P < 0.01$, *** $P < 0.001$ (Student's t test with Welch's correction); # $P < 0.05$, ## $P < 0.01$ versus GR-treated Con or saline-treated GFAP-Rs1 (Bonferroni test). Data are presented as mean \pm s.e.m.

a result of low *GFAP* promoter activity in early adulthood³³. In the Cornu Ammonis areas of the hippocampus, $12.46 \pm 1.83\%$ of *GFAP*-positive cells were immunoreactive for FLAG-Rs1 ($n = 16$ hippocampal sections from 6 mice). Similarly sparse and astrocyte-selective transgene expression was reported for the *GFAP-tTA* construct when it was used in combination with a fluorescent reporter³². GFAP-Rs1 mice were viable, of normal weight, and displayed typical locomotor, exploratory, nociceptive and anxiety-related behaviors up to 19 months of age, the oldest age tested (Supplementary Fig. 6e–k).

To determine whether activation of astrocytic G_s-coupled receptors affects learning and memory, we used the synthetic Rs1 ligand GR-125487, which activates Rs1, but not wild-type 5HT₄ receptors. In Rs1-expressing cultured astrocytes, GR-125487 increased the levels of cAMP and activated cAMP-linked downstream mediators, including ERK and CREB, but did not affect calcium levels (Fig. 4a–e), confirming that GR-125487 induces G_s-coupled, but not G_q-coupled, signaling. GR-125487 increased cAMP to similar levels as stimulation of

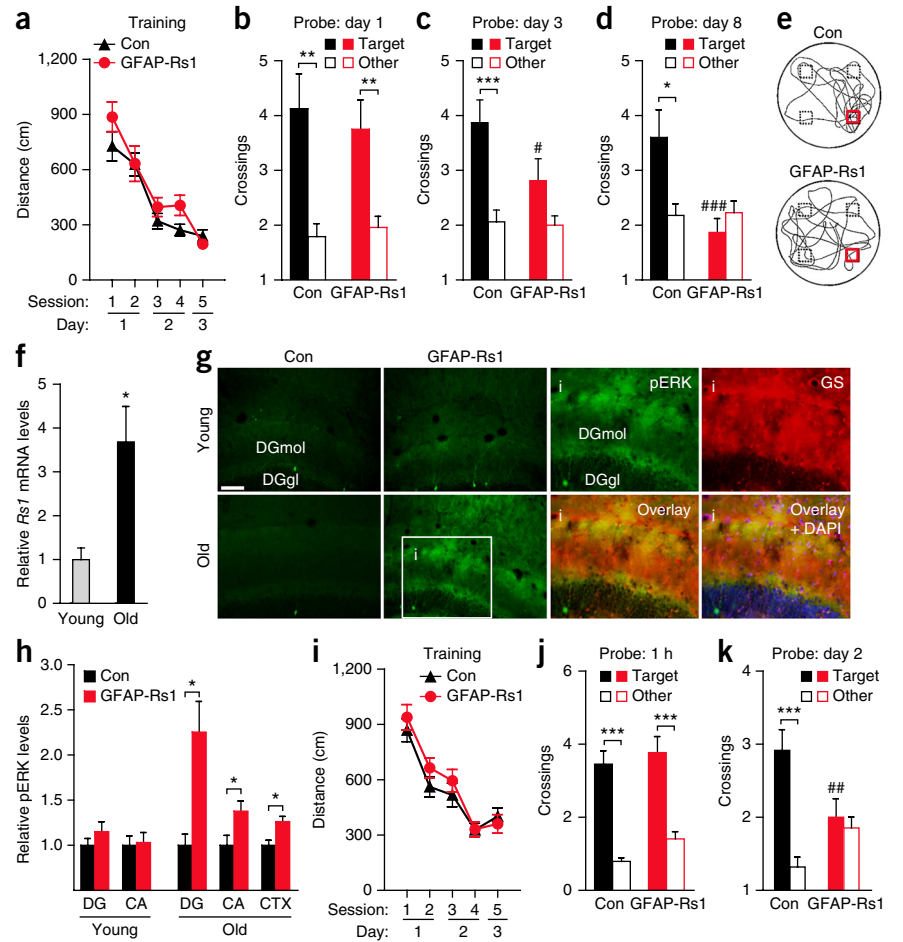


endogenous G_s-coupled prostaglandin receptors with PGE₂ (Fig. 4a), suggesting that Rs1 activation increases G_s-coupled signaling in a physiological range. In complementary *in vivo* experiments, we established that GR-125487 crossed the blood-brain barrier within minutes of intraperitoneal (i.p.) injection, achieved maximal concentrations in the brain within 30 min and exhibited a short half-life (Fig. 4f). In GFAP-Rs1 mice, but not in controls, phosphorylated ERK levels were increased in the hippocampal formation, but not cortex, 1 h after ligand injection and returned to baseline within 6 h (Fig. 4g).

Astrocytic G_s-coupled signaling reduces memory

The relatively rapid brain entry and clearance of the Rs1 ligand made it possible to test the effects of astrocytic G_s-coupled signaling on different stages of spatial learning and memory in the Morris water maze. The doubly transgenic GFAP-Rs1 mice and their littermate controls were generated on an F1 hybrid background consisting of 50% C57BL/6J and 50% FVB/N. Such hybrid mice perform better in the

Figure 6 Untreated young and aging GFAP-Rs1 mice have reduced memory. **(a–e)** Untreated GFAP-*tTA* (Con) and GFAP-Rs1 mice were tested in the Morris water maze at 5–7 months of age. **(a)** Distance traveled to reach the platform during hidden platform training. Two-way ANOVA: $F(4, 120) = 1.00$, $P = 0.41$ for interaction effect. $n = 16$ mice per genotype. **(b–d)** Crossings of the target and equivalent non-target (other) locations during probe trials conducted at indicated times after training. Two-way ANOVA: **(b)** $F(1, 60) = 0.37$, $P = 0.54$ for interaction effect; **(c)** $F(1, 59) = 2.48$, $P = 0.12$ for interaction effect; **(d)** $F(1, 57) = 7.92$, $P = 0.007$ for interaction effect. $n = 16$ mice (**b, c**) and 15 mice (**d**) per genotype. Student's *t* test with Welch's correction (target versus other of matching genotype): **(b)** $P = 0.0028$ (Con), $P = 0.0055$ (GFAP-Rs1); **(c)** $P = 0.0009$ (Con), $P = 0.076$ (GFAP-Rs1); **(d)** $P = 0.018$ (Con), $P = 0.28$ (GFAP-Rs1). **(e)** Representative swim paths during the probe on day 8. Squares indicate target (red) and non-target (black) locations. **(f)** *Rs1* mRNA levels in the cortex of young (2–4 months) and old (18–22 months) GFAP-Rs1 mice. *Actb* (β -actin) mRNA served as a loading control. *Rs1/Actb* ratios were normalized to the average ratio in young mice. Student's *t* test with Welch's correction (young versus old): $P = 0.012$. $n = 10$ young and 9 old GFAP-Rs1 mice. **(g)** Representative photomicrographs of pERK-immunostained (green) brain sections of young (2–5 months) and old (18–22 months) Con and GFAP-Rs1 mice. $n = 2$ young Con, 2 young GFAP-Rs1, 2 old Con and 8 old GFAP-Rs1 mice. Scale bar represents 100 μ m. Inset (**i**), magnified view of the boxed region co-immunostained for glutamine synthetase (GS, red) and cell nuclei (blue). DGmol, dentate gyrus (DG) molecular layer; DGgl, dentate gyrus granular layer. **(h)** Levels of phosphorylated ERK in different brain regions of Con and GFAP-Rs1 mice. Densitometric quantification of pERK/tERK ratios in the DG and CA regions of the hippocampus and in the cortex (CTX) of young (2–5 months) and old (18–22 months) mice. pERK/tERK ratios were normalized to the average ratio within each brain region of Con mice. $n = 6$ young/Con/DG, 6 young/GFAP-Rs1/DG, 6 young/Con/CA, 6 young/GFAP-Rs1/CA, 5 old/Con/DG, 11 old/GFAP-Rs1/DG, 6 old/Con/CA, 10 old/GFAP-Rs1/CA, 6 old/Con/CTX and 5 old/GFAP-Rs1/CTX mice. Student's *t* test with Welch's and FDR corrections (Con versus GFAP-Rs1): $P = 0.0138$ (DG), $P = 0.043$ (CA), $P = 0.018$ (CTX). **(i–k)** Untreated Con and GFAP-Rs1 mice were tested in the Morris water maze at 14–18 months of age. **(i)** Distance traveled to reach the platform during hidden platform training. Two-way ANOVA: $F(4, 192) = 0.60$, $P = 0.66$ for interaction effect. $n = 28$ Con and 22 GFAP-Rs1 mice. **(j, k)** Crossings during probe trials conducted at indicated times after completion of training. Two-way ANOVA: **(j)** $F(1, 46) = 0.25$, $P = 0.62$ for interaction effect, $n = 11$ Con and 13 GFAP-Rs1 mice; **(k)** $F(1, 90) = 12.27$, $P = 0.0007$ for interaction effect, $n = 26$ Con and 21 GFAP-Rs1 mice. Student's *t* test with Welch's correction (target versus other of matching genotype): **(j)** $P < 0.0001$ (Con), $P = 0.0002$ (GFAP-Rs1); **(k)** $P = 0.0002$ (Con), $P = 0.616$ (GFAP-Rs1). * $P < 0.05$, ** $P < 0.01$, *** $P < 0.001$ (Student's *t* test with Welch's correction). # $P < 0.05$, ## $P < 0.01$, ### $P < 0.001$ versus Con (Bonferroni test). Data are presented as mean \pm s.e.m.



Morris water maze than congenic C57BL/6J mice³⁴. Thus, the hybrid mice underwent only 2 d of hidden platform training in the Morris water maze (two sessions per day and two trials per session) before testing in probe trials. On each day of training, mice received a single injection of GR-125487 (3 mg per kg of body weight, i.p.) or saline 15 min before training (Fig. 5a). The daily training took 30 min or less to complete, coincident with peak brain ligand concentrations (Fig. 4f). One probe trial was performed 2 d after completion of training.

Ligand exposure during training did not interfere with task acquisition (learning) in GFAP-Rs1 or singly transgenic GFAP-*tTA* control mice (Fig. 5b). However, it impaired the performance of GFAP-Rs1 mice in a probe trial carried out 2 d after training (Fig. 5c). In contrast, saline-treated GFAP-Rs1 mice and ligand-treated control mice performed at the level of saline-treated controls (Fig. 5c). Swim speeds during the probe trial were comparable among all four groups (Supplementary Fig. 7a). 3 d after the probe trial, ligand-treated mice

received a saline injection 15 min before being retrained to a different platform location in a new spatial context (Fig. 5d). Saline-treated GFAP-Rs1 and control mice had comparable learning curves and, importantly, performed equally well in a probe trial conducted 3 d after retraining (Fig. 5e,f). Thus, Rs1 ligand exposure during learning of the first platform location reduced memory in GFAP-Rs1 mice in a reversible manner.

The Rs1 ligand requires several hours to be fully cleared from the brain (Fig. 4f) and its functional effects may be delayed or persist after ligand clearance. Thus, ligand exposure during learning could affect memory by disrupting processes that occur after learning, such as memory consolidation, storage or retrieval. To assess this possibility, we tested whether GR-125487 administered 1 d after completion of training also impaired memory (Fig. 5g). Indeed, memory was reduced in GFAP-Rs1 mice, but not in control GFAP-*tTA* or *TetO-Rs1* mice, when probed a day after the post-training GR-125487 injection

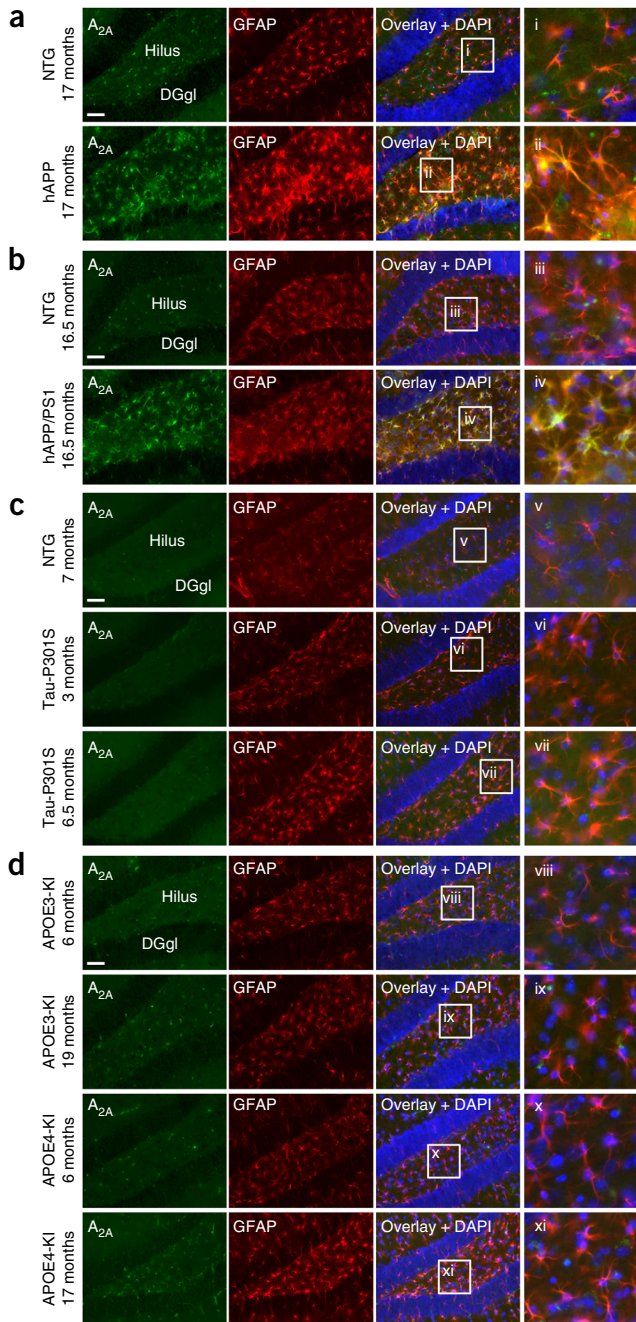
Figure 7 Astrocytic A_{2A} receptor levels are increased in transgenic mice expressing mutant forms of hAPP alone or in combination with a mutant form of PS1. **(a–d)** Representative photomicrographs of hippocampal sections immunostained for the A_{2A} receptor (green) and the astrocyte marker GFAP (red) from NTG mice and from transgenic mice expressing hAPP alone (**a**) or in combination with a mutant form of PS1 (**b**), transgenic mice expressing a mutant form of human tau (Tau-P301S) (**c**), or knock-in mice expressing human apoE3 (APOE3-KI) or apoE4 (APOE4-KI) (**d**). Ages of the mice are indicated in months (left). Cell nuclei were labeled with DAPI (blue). Insets (i–xi) show magnified views of the boxed regions. DGgl, dentate gyrus granular layer. *n* = 7 NTG and 8 hAPP mice (**a**); 3 NTG and 5 hAPP/PS1 mice (**b**); 1 NTG/7 months, 4 Tau-P301S/3 months and 4 Tau-P301S/6.5 months mice (**c**); 3 APOE3-KI/6 months, 3 APOE3-KI/19 months, 3 APOE4-KI/6 months and 3 APOE4-KI/17 months mice (**d**). Scale bars represent 50 μ m.

(Fig. 5h,i and Supplementary Fig. 7c–e). Swim speeds during this probe trial were comparable among all groups (Supplementary Fig. 7b). In contrast, the ligand did not affect memory retrieval when administered 2 d after training (Supplementary Fig. 7f,g). These results suggest that ligand-induced receptor activity in astrocytes might regulate the consolidation or storage of memory that can occur in less than 48 h after learning³⁵.

Constitutive astrocytic G_s-coupled activity reduces memory

In addition to its robust activation by synthetic ligands, Rs1 is known to exhibit ligand-independent constitutive G_s-coupled activity³¹. Consistent with these reports, Rs1-expressing cultured mouse astrocytes showed increased basal intracellular cAMP and phosphorylated CREB levels, but no increases in basal intracellular calcium levels (Supplementary Fig. 8a–d). To test whether this constitutive activity is sufficient to impair memory in GFAP-Rs1 mice, we tested untreated mice in the Morris water maze after increasing the delay between the completion of hidden platform training and the subsequent probe trials. Untreated GFAP-Rs1 mice learned well and showed robust memory in a probe trial conducted 1 d post-training (Fig. 6a,b). However, GFAP-Rs1 mice lost target preference by 8 d post-training (Fig. 6c–e). In contrast, control mice showed target preference on day 8 and lost target preference by day 15 post-training (Fig. 6d,e and Supplementary Fig. 8e). Untreated GFAP-Rs1 mice also showed reduced performance in a novel object-recognition task (Supplementary Fig. 8f,g), which depends on the ability to recall familiar objects, suggesting that the reduced memory in GFAP-Rs1 mice is not restricted to the Morris water maze or spatial memory tasks.

We also found that *Rs1* and *Gfap* mRNA levels increased with age (Fig. 6f and Supplementary Fig. 8h), likely as a result of age-dependent increases in the activity of the *Gfap* promoter²⁷. Basal levels of phosphorylated ERK were also higher in different brain regions of untreated 18–22-month-old GFAP-Rs1 mice than in age-matched singly transgenic controls and younger GFAP-Rs1 mice (Fig. 6g,h), suggesting increased constitutive astrocytic G_s-coupled signaling in aging GFAP-Rs1 mice. We therefore tested whether untreated GFAP-Rs1 mice develop more prominent memory loss as they age. Similar to younger GFAP-Rs1 mice, 14–18-month-old GFAP-Rs1 mice showed normal learning during hidden platform training (Fig. 6i) and normal short-term memory 1 h after training (Fig. 6j). However, the older GFAP-Rs1 mice lost target preference by 2 d post-training (Fig. 6k), whereas age-matched controls and younger GFAP-Rs1 mice showed normal memory at that time (Figs. 5c and 6k). These results suggest that age-dependent increases in the levels of constitutively active Rs1 are sufficient to reduce long-term memory. In contrast, working memory was normal in young and older GFAP-Rs1 mice (Supplementary Fig. 8i,j).



Astrocytic A_{2A} receptors are increased in aging hAPP mice

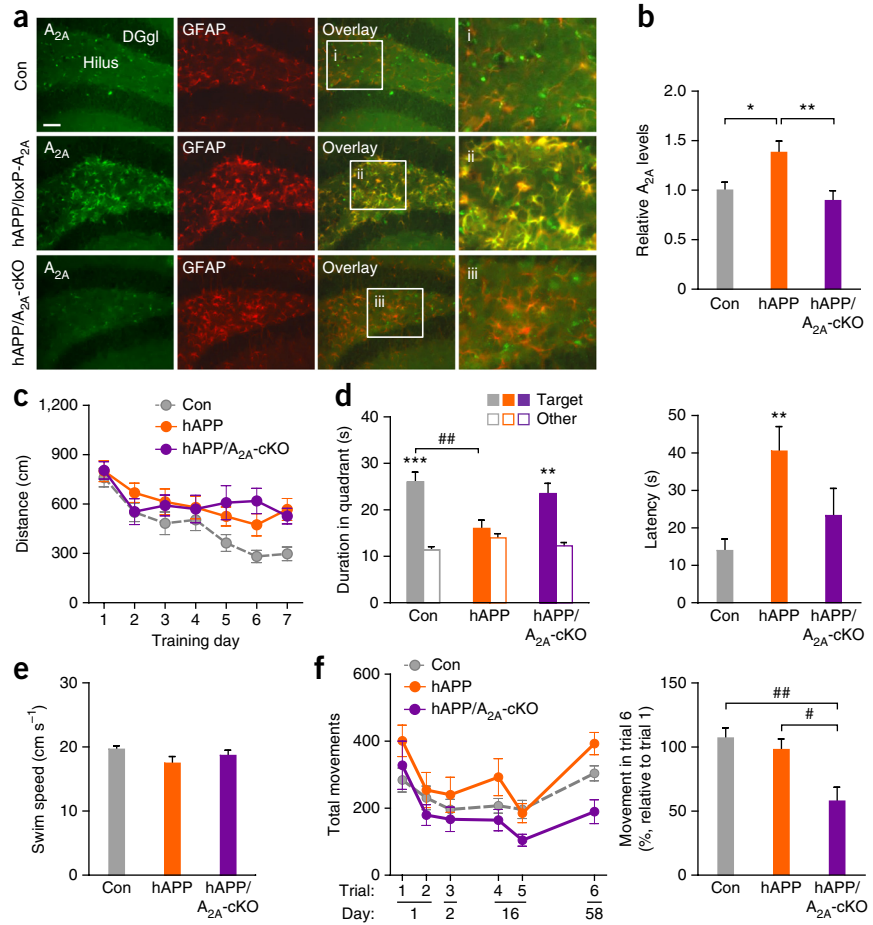
Our findings suggest that astrocytic A_{2A} receptors regulate memory in mice and that the levels of these receptors increase in humans with AD. We next investigated the link between AD pathology and astrocytic A_{2A} receptors in AD-related mouse models. Transgenic mice with neuronal expression of familial AD-linked mutant hAPP (hAPP mice) develop a number of AD-like pathological alterations, including amyloid plaques, neuritic dystrophy, astrocytosis and microgliosis, and show deficits in learning and memory^{10,36,37}. Also similar to humans with AD, we found that plaque-bearing 14–20-month-old hAPP mice from line J20 had increased levels of astrocytic A_{2A} receptor immunoreactivity in the hippocampus as compared with nontransgenic (NTG) littermate controls (Fig. 7a and Supplementary Figs. 9 and 10). The increases in A_{2A} receptor expression were localized to astrocytes, but not microglia, as determined by colabeling for the A_{2A} receptor and

Figure 8 Conditional ablation of A_{2A} receptors reduces memory deficits in aging hAPP mice. **(a,b)** Representative photomicrographs (**a**) and quantification (**b**) of A_{2A} receptor (green) immunostaining in hippocampal sections from 15–18-month-old *loxP-Adora2a* control mice (Con), *hAPP/loxP-Adora2a* mice (hAPP/loxp-A_{2A}), and *hAPP/loxP-Adora2a/Cre* mice (hAPP/A_{2A}-cKO). GFAP immunostaining is shown in red. Insets (i–iii) in **a** show magnified views of the boxed regions. DGgl, dentate gyrus granular layer. $n = 7$ Con, 6 hAPP/loxp-A_{2A} and 5 hAPP/A_{2A}-cKO mice. Scale bar represents 50 μ m.

(b) Quantification of A_{2A} receptor immunoreactivity in the hilus of the dentate gyrus. Levels were normalized to the average level in Con mice. One-way ANOVA: $F(2, 17) = 6.52$, $P = 0.0091$. $n = 7$ Con, 6 hAPP and 5 hAPP/A_{2A}-cKO mice. * $P < 0.05$, ** $P < 0.01$ versus hAPP (Bonferroni test). **(c–f)** hAPP mice with or without conditional ablation of astrocytic A_{2A} receptors were tested in the Morris water maze (**c–e**) and a habituation procedure involving repeated exposure to the same open field (**f**) at 15–17 months of age. **(c)** Distance traveled to reach the platform during hidden platform training (two trials per session, two sessions per day for 7 d). Two-way ANOVA revealed a significant difference between control (Con, singly transgenic *loxP-A_{2A}* mice) and hAPP mice ($F(1, 21) = 9.18$, $P = 0.0064$), but not between hAPP and hAPP/A_{2A}-cKO mice ($F(1, 16) = 0.01$, $P = 0.90$). $n = 14$ Con, 9 hAPP and 9 hAPP/A_{2A}-cKO mice. **(d)** Probe trial conducted 1 d after training in the Morris water maze. Left, durations in target and non-target (other) quadrants. One-way ANOVA: $F(2, 28) = 5.39$, $P = 0.0104$; one-sample *t* test versus chance duration of 15 s with FDR correction for multiple comparisons (target versus chance): $P = 0.0006$ (Con), $P = 0.618$ (hAPP), $P = 0.0054$ (hAPP/A_{2A}-cKO). $n = 14$ Con, 8 hAPP and 9 hAPP/A_{2A}-cKO mice. ** $P < 0.01$ versus Con (Dunnett's test); ** $P < 0.01$, *** $P < 0.001$ (one-sample *t* test). Right, latency to reach target location. One-way ANOVA: $F(2, 28) = 6.30$, $P = 0.0055$. ** $P < 0.01$ versus Con (Dunnett's test). $n = 14$ Con, 8 hAPP and 9 hAPP/A_{2A}-cKO mice. **(e)** Swim speeds during the probe trial. One-way ANOVA: $F(2, 28) = 2.28$, $P = 0.12$. $P > 0.05$ versus Con (Dunnett's test). $n = 14$ Con, 8 hAPP and 9 hAPP/A_{2A}-cKO mice. **(f)** Open-field habituation. Left, mice were habituated to the open field in 5-min trials (1–2 trials per day) for 2 d and tested in the same arena on days 16 and 58. Repeated measures two-way ANOVA: $F(2, 27) = 5.17$, $P = 0.0125$ for genotype effect, $F(5, 135) = 11.25$, $P < 0.0001$ for time effect, $F(10, 135) = 1.25$, $P = 0.27$ for interaction between genotype and time. Right, extent of dishabituation on day 58 (test trial 6 relative to trial 1). One-way ANOVA: $F(2, 27) = 7.94$, $P = 0.0019$. $n = 14$ Con, 8 hAPP and 8 hAPP/A_{2A}-cKO mice. # $P < 0.05$, ## $P < 0.01$ versus Con (Dunnett's test). Data are presented as mean \pm s.e.m.

cell-selective markers (Fig. 7a and Supplementary Figs. 9 and 10). The most prominent increases in astrocytic A_{2A} receptor expression were found in the vicinity of thioflavin-S-positive plaques (Supplementary Fig. 9d,e). In contrast with aging hAPP mice, 2–3-month-old hAPP mice had no plaques³⁶ and showed no increases in astrocytic A_{2A} receptor immunoreactivity (Supplementary Fig. 10a).

We also found increases in astrocytic A_{2A} receptor levels in plaque-bearing 16.5-month-old doubly transgenic mice expressing mutant hAPP and human presenilin 1 (hAPP/PS1 mice)³⁸ (Fig. 7b), indicating that this alteration is not unique to hAPP mice from line J20. We also examined 6.5-month-old mice expressing a mutant form of human tau (Tau-P301S), which causes astrogliosis, axonal degeneration and synaptic loss by 6 months of age³⁹. Notably, these mice did not show increases in A_{2A} receptor expression at this age (Fig. 7c). Astrocytic A_{2A} receptor levels also did not increase in 17-month-old mice expressing human apolipoprotein E4 (*APOE4* knock-in mice⁴⁰; Fig. 7d). These results suggest that pathological accumulation of A β , but not tauopathy or the inheritance of the *APOE4* gene, contributes to the increased astrocytic A_{2A} receptor levels that we observed in post-mortem brain tissues from humans with sporadic AD (Fig. 1).



The expression of mutant forms of tau and ApoE4 might induce an astrocytic response that is different in nature or lower in magnitude than the astrocytic response to A β accumulation.

To further address the specificity of this astrocytic response, we tested whether astrocytic A_{2A} receptor levels also increase in acute neuropathological conditions. In particular, we assessed wild-type mice after kainate-induced excitotoxicity. Prominent increases in the levels of astrocytic A_{2A} receptors were detected 3 and 7 d after a single injection of kainate (30 mg per kg, i.p.; Supplementary Fig. 11). Thus, increases in astrocytic A_{2A} receptor levels are not unique to AD-linked pathology and may occur in other neuropathological conditions associated with astrogliosis.

Astrocytic A_{2A} receptors promote memory loss in hAPP mice

We next tested whether astrocytic A_{2A} receptors contribute to memory deficits in aging hAPP mice. We generated transgenic mice expressing hAPP with or without conditional ablation of astrocytic A_{2A} receptors (Fig. 8a,b) and tested these mice in the Morris water maze and the open field. Specifically, we tested three groups of transgenic mice: singly transgenic control mice carrying two *loxP-Adora2a*

alleles, doubly transgenic hAPP mice carrying human *APP* and one or two *loxP-Adora2a* alleles, and triply transgenic hAPP/A_{2A}-cKO mice carrying human *APP*, two *loxP-Adora2a* alleles and Cre recombinase. Ablation of astrocytic A_{2A} receptors did not affect the learning deficits of 15–17-month-old hAPP mice during hidden platform training (Fig. 8c), consistent with our observations that ablation of these receptors does not affect learning in young and aging mice without hAPP expression (Fig. 2). Notably, ablation of astrocytic A_{2A} receptors enhanced the performance of hAPP mice in a probe trial 24 h after training (Fig. 8d). Specifically, hAPP mice bearing astrocytic A_{2A} receptors showed a minimal preference for the target quadrant and an increased latency to reach the platform location compared with singly transgenic control mice without hAPP expression. In contrast, hAPP/A_{2A}-cKO mice showed a clear preference for the target quadrant and a lower latency to reach the platform location. Swim speeds during the probe trial were comparable among the groups (Fig. 8e). Moreover, hAPP/A_{2A}-KO mice showed less dishabituation in the open field than hAPP mice and singly transgenic controls (Fig. 8f), consistent with our findings in A_{2A}-cHET and A_{2A}-cKO mice without hAPP expression (Fig. 2c–f).

Ablation of astrocytic A_{2A} receptors did not affect memory deficits or other cognitive impairments in hAPP mice tested at younger ages, when the levels of astrocytic A_{2A} receptors were not yet increased (Supplementary Fig. 12). Together, our results suggest that astrocytic A_{2A} receptors regulate memory and that aberrant increases in the expression of these receptors in aging hAPP mice contribute to memory deficits.

DISCUSSION

Astrocytes influence diverse aspects of brain function and likely influence cognitive processes such as learning and memory^{41,42}. Indeed, astrocytes release transmitters that modulate synaptic plasticity⁴³, a process that is crucial for learning and memory. Astrocytes might also regulate learning and memory by releasing lactate or other metabolic substrates that support neuronal functions⁴². However, oligodendrocytes similarly release lactate, which supports neuronal functions, and it remains to be determined which cell type mediates the effects of lactate on memory⁴⁴. Indeed, the specific roles of astrocytes in learning and memory remain unclear.

Here we provide evidence that astrocytic G_s-coupled receptor activity can regulate memory. Chronic or acute increases in astrocytic G_s-coupled receptor activity reduced memory, whereas astrocytic reduction or ablation of the G_s-coupled A_{2A} receptors enhanced memory in young and aging mice without hAPP expression, and in aging mice with hAPP expression. In contrast, we did not detect changes in learning, working memory, short-term memory or other behavioral functions. Together, these results suggest that astrocytic G_s-coupled receptors regulate memory retention or consolidation. In further support of this notion, prolonging the time between memory acquisition and retrieval amplified the effects observed in GFAP-Rs1, A_{2A}-cHET and A_{2A}-cKO mice, and ligand injection after training was sufficient to worsen memory in GFAP-Rs1 mice.

In the *GFAP-Cre/loxP-Adora2a* mice, widespread ablation of astrocytic A_{2A} receptors was achieved by *GFAP* promoter-driven Cre, as reported previously for *Adora2a* and other *loxP*-flanked genes^{7,20}. However, we detected sparse astrocytic expression of Rs1 in GFAP-Rs1 mice, as observed when the *GFAP-tTA* construct was used in combination with a fluorescent reporter³². Astrocytes form a highly interconnected syncytium as a result of cell-to-cell gap junctions, which are permeable to various signaling factors⁴⁵. It is therefore conceivable that increased G_s-coupled signaling in a relatively small

proportion of astrocytes could result in more widespread changes in astrocytic activities and have a dominant gain-of-function effect on memory retention.

The levels of astrocytic Rs1 expression and activation may be amenable to titration, for example, by adjusting the dose and duration of ligand treatment, introducing other astrocytic promoters to control Rs1 expression, or using mutagenesis to alter the properties of Rs1 activation and desensitization. In regards to the acute experiments, the main disadvantage of this chemogenetic system is the constitutive activity of the receptor in the absence of ligand. However, the constitutive activity was informative in our long-term studies, as it allowed us to demonstrate the effects of chronic receptor activation on behavior. Off-target effects of the Rs1 ligand could be another disadvantage of this system, but we did not find any biochemical or behavioral evidence for such effects.

Despite the many differences between the two transgenic systems, we found consistent effects on memory and these effects were observed across different ages, behavioral procedures and chemogenetic conditions. The effects on memory were also observed in the presence of hAPP/A β -induced pathology. Notably, astrocytic A_{2A} receptor ablation enhanced memory in older hAPP mice that had abundant amyloid plaques and increased levels of astrocytic A_{2A} receptors, but not in young hAPP mice that had no or minimal plaques and unaltered levels of these receptors. These results suggest that the pathogenic mechanisms causing memory deficits in young versus aging hAPP mice may be at least partly distinct. In particular, plaque-associated alterations in astrocytic A_{2A} receptors, and possibly changes in other astrocytic functions, likely contribute to memory deficits in aging hAPP mice. Alternative pathogenic mechanisms that are independent of astrocytic A_{2A} receptors¹⁰ probably cause learning/memory deficits in young hAPP mice. These mechanisms may have offset or prevented any improvements in memory one might expect the astrocytic A_{2A} ablation to have caused based on our findings in young mice without hAPP expression. It is tempting to speculate that distinct pathogenic mechanisms may also predominate at different stages of AD and may require distinct therapeutic interventions to reduce memory deficits.

Ablation of astrocytic A_{2A} receptors likely modulates memory by preventing endogenous adenosine from activating these receptors¹. Notably, adenosine levels can increase markedly during intense neuronal activity, metabolic dysfunction or prolonged wakefulness⁴⁶. Astrocytic A_{2A} receptors could have more prominent effects on memory under these conditions. Notably, if the levels of astrocytic A_{2A} receptors increase, as we found to occur in humans with AD and in mice with amyloid plaques or excitotoxic injury, then even low levels of adenosine might be sufficient to cause prominent effects on memory. Indeed, our results in GFAP-Rs1 mice suggest that increases in the activity or expression of astrocytic G_s-coupled receptors can reduce memory.

Together, our findings suggest that astrocytic A_{2A} receptors regulate memory under physiological conditions and can have aberrant effects on memory under pathophysiological conditions. Although A_{2A} receptors have previously been implicated in AD pathogenesis^{8,9}, the roles of astrocytic A_{2A} receptors in this condition were not known. Our findings suggest that AD causes increases in astrocytic A_{2A} receptors that can regulate memory and that targeting these receptors might be a therapeutic strategy for memory enhancement. However, these receptors are expressed throughout the body and altering their activity in a nonselective manner might cause a variety of effects. This caveat notwithstanding, caffeine, which nonselectively blocks adenosine receptors A₁ and A_{2A}¹, is remarkably safe and enhances memory in humans⁴⁷. However, the cellular and molecular substrates of these cognitive effects are not known.

To the best of our knowledge, the roles of astrocytic G_s-coupled receptors in behavior and cognitive functions have not been previously investigated. Our study therefore provides the first evidence that astrocytic G_s-coupled receptors regulate memory. In particular, our findings raise the possibility that this astrocytic signaling pathway regulates the processes underlying memory storage or consolidation. A nonexclusive possibility is that it forms part of an active process that promotes forgetting⁴⁸. Astrocytes are multi-functional cells with pleiotropic effects on neuronal structure and function. Conceivably, astrocytic G_s-coupled signaling regulates astrocytic-neuronal interactions that in turn modulate memory-linked processes, such as synaptic plasticity and neural network activity. Although the mechanisms by which astrocytic G_s-coupled signaling influences these or related memory processes remain to be determined, this signaling pathway has been linked to a variety of intracellular effects in astrocytes, including changes in gene transcription, cytoskeletal remodeling and glutamate transport^{7,49,50}. Alterations in one or more of these astrocytic functions might modulate memory-linked processes. Because G protein-coupled receptors are attractive drug targets, further elucidating their roles in astrocytic functions and memory processing could have therapeutic implications for AD and other conditions that involve astrocytosis and memory loss.

METHODS

Methods and any associated references are available in the [online version of the paper](#).

Note: Any Supplementary Information and Source Data files are available in the online version of the paper.

ACKNOWLEDGMENTS

We thank P.E. Sanchez for advice on behavioral experiments, R. Ponnusamy for comments on the manuscript, J.-F. Chen (Boston University School of Medicine) for providing loxP-Adora2a transgenic mice, N. Déglon (Lausanne University Hospital) for providing the lentiviral vector and packaging plasmids, B. Khakh (University of California, Los Angeles) for providing the plasmid encoding the membrane-targeting region of lck, S.-W. Min and L. Gan (Gladstone Institute of Neurological Disease) for providing brain tissue from *Tau-P301S* mice, L. Leung and Y. Huang (Gladstone Institute of Neurological Disease) for providing brain tissue from *ApoE3-KI* and *ApoE4-KI* mice, A. Lundquist, G. Shlager, C. Wang and E. Whiting for technical support, R. Craft, T. Hamto, I. Lo and B. Masatsugu of the Gladstone Behavioral Core for advice and technical support, and M. Dela Cruz and A. Cheung for administrative assistance. This study was supported by US National Institutes of Health grants AG039220 to A.G.O., AR056299 to E.C.H., AG034531 to D.B.D. HL60664 and HL100406 to B.R.C., and AG022074 and NS065780 to L.M., and a MetLife Foundation Award to L.M. The Gladstone Institutes received support from a National Center for Research Resources Grant RR18938.

AUTHOR CONTRIBUTIONS

A.G.O. and L.M. designed and coordinated the study. A.G.O. carried out *in vitro* assays, immunohistochemistry, western blotting and behavioral testing. E.C.H. and B.R.C. generated *TetO-Rs1* transgenic mice and the plasmids encoding Rs1 and provided advice on Rs1 ligands. M.M.W. helped to conduct and analyze behavioral tests. K.H. performed western blotting, immunoprecipitation, immunohistochemistry and mouse perfusions. D.H.K. and D.B.D. performed qRT-PCR. X.W. administered drugs and genotyped and perfused mice. W.G., J.K. and G.-Q.Y. managed mouse lines and performed mouse perfusions. A.A. and E.M. performed immunohistochemistry, helped analyze related data and provided human tissue. N.D. helped design and conduct behavioral tests. A.G.O. and L.M. wrote the manuscript.

COMPETING FINANCIAL INTERESTS

The authors declare no competing financial interests.

Reprints and permissions information is available online at <http://www.nature.com/reprints/index.html>.

1. Fredholm, B.B., IJzerman, A.P., Jacobson, K.A., Klotz, K.N. & Linden, J. International Union of Pharmacology. XXV. Nomenclature and classification of adenosine receptors. *Pharmacol. Rev.* **53**, 527–552 (2001).

2. Burnstock, G. Physiology and pathophysiology of purinergic neurotransmission. *Physiol. Rev.* **87**, 659–797 (2007).
3. Bogenpohl, J.W., Ritter, S.L., Hall, R.A. & Smith, Y. Adenosine A2A receptor in the monkey basal ganglia: ultrastructural localization and colocalization with the metabotropic glutamate receptor 5 in the striatum. *J. Comp. Neurol.* **520**, 570–589 (2012).
4. Chen, J.F. et al. Adenosine A2A receptors and brain injury: broad spectrum of neuroprotection, multifaceted actions and “fine tuning” modulation. *Prog. Neurobiol.* **83**, 310–331 (2007).
5. Saura, J. et al. Adenosine A2A receptor stimulation potentiates nitric oxide release by activated microglia. *J. Neurochem.* **95**, 919–929 (2005).
6. Orr, A.G., Orr, A.L., Li, X.J., Gross, R.E. & Traynelis, S.F. Adenosine A(2A) receptor mediates microglial process retraction. *Nat. Neurosci.* **12**, 872–878 (2009).
7. Matos, M., Augusto, E., Agostinho, P., Cunha, R.A. & Chen, J.F. Antagonistic interaction between Adenosine A2A receptors and Na⁺/K⁺-ATPase-alpha2 controlling glutamate uptake in astrocytes. *J. Neurosci.* **33**, 18492–18502 (2013).
8. Albasanz, J.L., Perez, S., Barrachina, M., Ferrer, I. & Martin, M. Up-regulation of adenosine receptors in the frontal cortex in Alzheimer’s disease. *Brain Pathol.* **18**, 211–219 (2008).
9. Laurent, C. et al. A2A adenosine receptor deletion is protective in a mouse model of Tauopathy. *Mol. Psychiatry* published online, doi:10.1038/mp.2014.151 (2 December 2014).
10. Huang, Y. & Mucke, L. Alzheimer mechanisms and therapeutic strategies. *Cell* **148**, 1204–1222 (2012).
11. Heneka, M.T. & O’Banion, M.K. Inflammatory processes in Alzheimer’s disease. *J. Neuroimmunol.* **184**, 69–91 (2007).
12. Braak, H. & Braak, E. Staging of Alzheimer’s disease-related neurofibrillary changes. *Neurobiol. Aging* **16**, 271–278 (1995).
13. Cahoy, J.D. et al. A transcriptome database for astrocytes, neurons and oligodendrocytes: a new resource for understanding brain development and function. *J. Neurosci.* **28**, 264–278 (2008).
14. Pickel, V.M., Chan, J., Linden, J. & Rosin, D.L. Subcellular distributions of adenosine A1 and A2A receptors in the rat dorsomedial nucleus of the solitary tract at the level of the area postrema. *Synapse* **60**, 496–509 (2006).
15. Lazarus, M. et al. Arousal effect of caffeine depends on adenosine A2A receptors in the shell of the nucleus accumbens. *J. Neurosci.* **31**, 10067–10075 (2011).
16. Bajenaru, M.L. et al. Astrocyte-specific inactivation of the neurofibromatosis 1 gene (NF1) is insufficient for astrocytoma formation. *Mol. Cell. Biol.* **22**, 5100–5113 (2002).
17. Fox, I.J. et al. Developmental expression of glial fibrillary acidic protein mRNA in mouse forebrain germinal zones: implications for stem cell biology. *Brain Res. Dev. Brain Res.* **153**, 121–125 (2004).
18. Karasinska, J.M. et al. ABCA1 influences neuroinflammation and neuronal death. *Neurobiol. Dis.* **54**, 445–455 (2013).
19. Stenzel, D. et al. Integrin-dependent and -independent functions of astrocytic fibronectin in retinal angiogenesis. *Development* **138**, 4451–4463 (2011).
20. Yamanaka, K. et al. Astrocytes as determinants of disease progression in inherited amyotrophic lateral sclerosis. *Nat. Neurosci.* **11**, 251–253 (2008).
21. Garcia, A.D., Doan, N.B., Imura, T., Bush, T.G. & Sofroniew, M.V. GFAP-expressing progenitors are the principal source of constitutive neurogenesis in adult mouse forebrain. *Nat. Neurosci.* **7**, 1233–1241 (2004).
22. Matos, M. et al. Adenosine A2A receptors modulate glutamate uptake in cultured astrocytes and gliosomes. *Glia* **60**, 702–716 (2012).
23. Rebola, N., Lujan, R., Cunha, R.A. & Mulle, C. Adenosine A2A receptors are essential for long-term potentiation of NMDA-EPSCs at hippocampal mossy fiber synapses. *Neuron* **57**, 121–134 (2008).
24. Vianna, M.R. et al. Role of hippocampal signaling pathways in long-term memory formation of a nonassociative learning task in the rat. *Learn. Mem.* **7**, 333–340 (2000).
25. Ledent, C. et al. Aggressiveness, hypoalgesia and high blood pressure in mice lacking the adenosine A2a receptor. *Nature* **388**, 674–678 (1997).
26. Bastia, E. et al. A crucial role for forebrain adenosine A(2A) receptors in amphetamine sensitization. *Neuropsychopharmacology* **30**, 891–900 (2005).
27. O’Callaghan, J.P. & Miller, D.B. The concentration of glial fibrillary acidic protein increases with age in the mouse and rat brain. *Neurobiol. Aging* **12**, 171–174 (1991).
28. Wimmer, M.E., Hernandez, P.J., Blackwell, J. & Abel, T. Aging impairs hippocampus-dependent long-term memory for object location in mice. *Neurobiol. Aging* **33**, 2220–2224 (2012).
29. Plath, N. et al. Arc/Arg3.1 is essential for the consolidation of synaptic plasticity and memories. *Neuron* **52**, 437–444 (2006).
30. Alexander, G.M. et al. Remote control of neuronal activity in transgenic mice expressing evolved G protein-coupled receptors. *Neuron* **63**, 27–39 (2009).
31. Chang, W.C. et al. Modifying ligand-induced and constitutive signaling of the human 5-HT4 receptor. *PLoS ONE* **2**, e1317 (2007).
32. Halassa, M.M., Fellin, T., Takano, H., Dong, J.H. & Haydon, P.G. Synaptic islands defined by the territory of a single astrocyte. *J. Neurosci.* **27**, 6473–6477 (2007).
33. Bai, X. et al. Genetic background affects human glial fibrillary acidic protein promoter activity. *PLoS ONE* **8**, e66873 (2013).
34. Han, H.J. et al. Strain background influences neurotoxicity and behavioral abnormalities in mice expressing the tetracycline transactivator. *J. Neurosci.* **32**, 10574–10586 (2012).

35. Tse, D. *et al.* Schemas and memory consolidation. *Science* **316**, 76–82 (2007).
36. Mucke, L. *et al.* High-level neuronal expression of A β _{1–42} in wild-type human amyloid protein precursor transgenic mice: synaptotoxicity without plaque formation. *J. Neurosci.* **20**, 4050–4058 (2000).
37. Ji, B. *et al.* Imaging of peripheral benzodiazepine receptor expression as biomarkers of detrimental versus beneficial glial responses in mouse models of Alzheimer's and other CNS pathologies. *J. Neurosci.* **28**, 12255–12267 (2008).
38. Jankowsky, J.L. *et al.* Mutant presenilins specifically elevate the levels of the 42 residue beta-amyloid peptide *in vivo*: evidence for augmentation of a 42-specific gamma secretase. *Hum. Mol. Genet.* **13**, 159–170 (2004).
39. Yoshiyama, Y. *et al.* Synapse loss and microglial activation precede tangles in a P301S tauopathy mouse model. *Neuron* **53**, 337–351 (2007).
40. Sullivan, P.M. *et al.* Targeted replacement of the mouse apolipoprotein E gene with the common human *APOE3* allele enhances diet-induced hypercholesterolemia and atherosclerosis. *J. Biol. Chem.* **272**, 17972–17980 (1997).
41. Han, J. *et al.* Acute cannabinoids impair working memory through astroglial CB1 receptor modulation of hippocampal LTD. *Cell* **148**, 1039–1050 (2012).
42. Suzuki, A. *et al.* Astrocyte-neuron lactate transport is required for long-term memory formation. *Cell* **144**, 810–823 (2011).
43. Panatier, A. *et al.* Glia-derived D-serine controls NMDA receptor activity and synaptic memory. *Cell* **125**, 775–784 (2006).
44. Lee, Y. *et al.* Oligodendroglia metabolically support axons and contribute to neurodegeneration. *Nature* **487**, 443–448 (2012).
45. Altevogt, B.M. & Paul, D.L. Four classes of intercellular channels between glial cells in the CNS. *J. Neurosci.* **24**, 4313–4323 (2004).
46. Dunwiddie, T.V. & Masino, S.A. The role and regulation of adenosine in the central nervous system. *Annu. Rev. Neurosci.* **24**, 31–55 (2001).
47. Borota, D. *et al.* Post-study caffeine administration enhances memory consolidation in humans. *Nat. Neurosci.* **17**, 201–203 (2014).
48. Hardt, O., Nader, K. & Nadel, L. Decay happens: the role of active forgetting in memory. *Trends Cogn. Sci.* **17**, 111–120 (2013).
49. Goldman, J.E. & Abramson, B. Cyclic AMP-induced shape changes of astrocytes are accompanied by rapid depolymerization of actin. *Brain Res.* **528**, 189–196 (1990).
50. Murray, P.D., Kingsbury, T.J. & Krueger, B.K. Failure of Ca²⁺-activated, CREB-dependent transcription in astrocytes. *Glia* **57**, 828–834 (2009).

ONLINE METHODS

Mice. Mice were housed in the Gladstone Institutes' animal facility and treated in accordance with guidelines set by the Institutional Animal Care and Use Committee of the University of California, San Francisco. Mice were housed in groups of 2–5 mice per cage and maintained on a 12-h light/dark cycle with *ad libitum* access to food and water. Mice tested in the Morris water maze were single-housed for the duration of the experiment. All experiments were conducted during the light cycle and included littermate controls.

GFAP-Cre/loxP-Adora2a transgenic mice were generated by crossing *GFAP-Cre* transgenic mice¹⁶ (C57BL/6) with *loxP-Adora2a* transgenic mice¹⁵ (C57BL/6, kindly provided by J.-F. Chen, Boston University). Global homozygous A_{2A} receptor knockout mice⁵¹ (A_{2A}-gKO, also known as *Adora2a*^{-/-}, 129S-*Adora2a*^{tm1f}/J, 129S4/SvJae × BALB/cJ, Jackson Laboratory) were used as a negative control for immunohistochemical analyses.

Regulatable Tet-off doubly transgenic GFAP-Rs1 mice were generated by crossing *GFAP-tTA* transgenic mice (C57BL/6, Jackson Laboratory) with *TetO-Rs1* transgenic mice (FVB/N). *GFAP-tTA* mice express the tetracycline transactivator (tTA) downstream of the human glial fibrillary acidic protein (GFAP) promoter⁵². *TetO-Rs1* mice possess a *Tet* operator (*TetO*)-driven FLAG-Rs1 transgene^{53,54}. The Rs1 receptor has an N-terminal FLAG tag to allow its detection by immunolabeling and western blotting. Doxycycline (DOX) administration in doubly transgenic GFAP-Rs1 mice blocks the binding of tTA to *TetO* and thereby prevents transgene expression. To prevent possible embryonic and postnatal developmental effects of Rs1, breeding pairs and offspring were maintained on DOX-supplemented chow (200 mg per kg of diet, Bio-Serv), unless indicated otherwise. Offspring were weaned at 3 weeks of age and thereafter maintained on DOX-free chow (Picolab Rodent Diet 20, Labdiet), unless indicated otherwise.

Previous studies utilizing *GFAP-tTA* mice to regulate *TetO*-driven transgenes have consistently shown transgene expression that is restricted to GFAP-positive astrocytes^{32,55–58}. However, a recent report suggested that GFAP-driven tTA can transactivate low-to-moderate levels of transgene expression in neurons in a line that combines four different transgenes⁵⁹. We agree with Fujita *et al.*⁵⁹ and others⁶⁰ that selective manipulation of astrocytic gene expression is a major technical challenge that requires careful validation of every new mouse line. We did not detect neuronal Rs1 expression in GFAP-Rs1 mice (Fig. 3 and Supplementary Fig. 6); however, we cannot exclude that Rs1 was expressed at very low levels in some neuronal populations in this model.

hAPP mice (C57BL/6, line J20) express an alternatively spliced human APP minigene encoding hAPP695, hAPP751 and hAPP770 with the Swedish and Indiana familial mutations regulated by the PDGF β-chain promoter^{36,61,62}. Some hAPP mice were crossed with *loxP-Adora2a* transgenic mice and the offspring were crossed with *GFAP-Cre/loxP-Adora2a* transgenic mice to generate *loxP-Adora2a* mice with or without hAPP and Cre expression. Doubly-transgenic hAPP/PS1 mice (C57BL/6, Jackson Laboratory) express a chimeric human/mouse APP695 with the Swedish mutation and a mutant human presenilin 1 (PS1-dE9) associated with familial AD under the control of mouse prion protein promoter elements³⁸. *Tau-P301S* mice (B6C3F1, The Jackson Laboratory) express a P301S mutant form of human tau under control of the mouse prion protein (*Prnp*) promoter and exhibit neurofibrillary tangles by 5 months of age³⁹. APOE3-KI and APOE4-KI mice (C57BL/6, Taconic) express human apoE3 or apoE4, respectively, in place of endogenous mouse apoE, under the control of endogenous mouse *ApoE* regulatory sequences^{40,63}. Because female mice show more prominent apoE4-induced neuronal impairments than male mice^{64,65}, only female mice were used to assess the effects of apoE4 on A_{2A} receptor expression.

Primary astrocyte cultures. Cortices and hippocampi from postnatal day 1–3 mouse pups (C57Bl/6, Jackson Laboratory) were isolated from the meninges and dissociated by trituration, plated into wells pre-coated with poly-D-lysine (50 µg ml⁻¹, Sigma-Aldrich), and maintained in DMEM supplemented with 15% FBS, 25 mM glucose, 2 mM L-glutamine and 1 mM sodium pyruvate (Life Technologies). Cells were washed after 4–5 d in culture and used in experiments after 6–15 d in culture. For assessment of phosphorylated protein levels by western blotting, the medium was replaced 18–24 h before agonist treatment with DMEM lacking serum and L-glutamine. The following agonists were used: prostaglandin E₂ (Cayman Chemical Company), adenosine 5'-triphosphate

(ATP, Sigma-Aldrich), forskolin (FSK, Calbiochem), GR-125487 (GR, Tocris), CGS-21680 (CGS, Sigma-Aldrich), or adenosine (Sigma-Aldrich).

Lentivirus preparation. The lentiviral vector backbone and three packaging plasmids⁶⁶ were provided by N. Déglon (Lausanne University Hospital). The Rs1 sequence was isolated from the pEntR3L2 *TetO-mCh-Rs1* plasmid^{31,54} and the mouse A_{2A} receptor sequence (*Adora2a*) from a SPORT6.1 plasmid (accession number: 30242398, Thermo Scientific). To generate the lentiviral vectors, PCR products encoding the mouse A_{2A} receptor, mCherry or mCherry with Rs1-FLAG separated by a sequence for the ribosomal skip site P2A were amplified using the Expand High Fidelity PCR system (Roche). The membrane-targeting region of lck^{67,68} (kindly provided by B. Khakh, University of California, Los Angeles) was inserted N-terminally of mCherry. The following primer sequences were used: Lck-forward, CATGGCTGTGGCTGCAGCTC; mCherry forward, ATGGTGAGCA AGGGCGAGGAGGATA; mCherry reverse, TTACTTGTACAGCTCGTCAT; Lck/mCherry forward, GCCATTATCCCATGGTGAGCA; Lck/mCherry reverse, TGCTCACCATGGATAATGGC; Rs1 reverse, CTAAGTGTCACTGGGCTG AGCAGC; *Adora2a* forward, ATGGGCTCTCGGTGTACATCATGGTGG; *Adora2a* reverse, TCAGGAAGGGGCAAACCTGAAGACCAT.

Amplified PCR products containing *Adora2a* (Lenti-A_{2A}), *lck-mCherry-P2A-Rs1* (Lenti-Rs1), or *lck-mCherry* (Lenti-mCherry) were inserted into the pCR8/GW/TOPO plasmid by TA cloning (Life Technologies) and transferred into the lentiviral vector backbone *SIN-cPPT-PGK-Gateway-WPRE-miR124T* using the Gateway LR Clonase II recombination system (Life Technologies). Lentiviral particles were generated by co-transfection of HEK293T cells with a transgene-encoding vector and three packaging plasmids (*pCMV-ΔR8.92*, *pRSV-Rev*, and *pGMokola*) using the CalPhos transfection kit (Clontech). Viral particles were purified from the culture medium by ultracentrifugation and resuspended in Hanks Balanced Salt Solution (HBSS). Viral titers were determined by p24 ELISA. Cells in 6-well plates or 96-well plates were transduced after 5–6 d in culture with lentiviral particles at 100 ng per well or 10 ng per well, respectively, or as indicated.

Drug administration. GR-125487 (Tocris) was dissolved in sterile 0.9% saline solution. For behavioral testing, mice were injected i.p. with 200 µl of GR-125487 in saline (3 mg per kg) or saline alone. Injections were performed by an experimenter who did not perform the behavioral experiments and was blinded to the treatment conditions and mouse genotypes.

To determine the pharmacokinetic profile of GR-125487 in the brain, 3–4-month-old nontransgenic C57BL/6 mice were injected i.p. with 1 mg per kg GR-125487 dissolved in sterile 0.9% saline. At different time points after injection, mice were anesthetized with Avertin (tribromoethanol, 250 mg per kg) and perfused transcardially with 0.9% saline for 1 min. Brains were removed and GR-125487 concentration in whole hemibrains was measured by Brains Online using HPLC with tandem mass spectrometry and internal standards.

Wild-type FVB/N/J mice (2–3 months old, Jackson Laboratory) were injected i.p. with 0.9% saline or kainic acid dissolved in saline (Sigma-Aldrich, 30 mg per kg). Within 10 min after injection of kainic acid, all mice showed subtle behavioral signs of epileptic activity, including immobility and head nodding. At different time points after injection, mice were anesthetized with Avertin (tribromoethanol, 250 mg per kg) and perfused transcardially with 0.9% saline for 1 min. Brains were removed and post-fixed in 4% PFA before immunohistochemical analyses.

Behavioral testing. For all behavioral experiments, experimenters were blinded as to the genotype and treatment of mice. Behavioral experiments in GFAP-Rs1 mice were conducted on F1 generation littermates at least four weeks after DOX removal (Supplementary Table 2). Littermates were randomly assigned to a treatment condition and groups were balanced for sex and age as closely as possible (Supplementary Table 2). Mice that showed poor health (for example, skin lesions, eye injury, tumors, slowed movement or inability to swim) were excluded from behavioral testing.

Morris water maze. The maze consisted of a 122-cm-diameter pool filled with water (20 ± 2 °C) made opaque with nontoxic white tempera paint. The pool was surrounded with distinct extra-maze cues. Before hidden platform training, all mice underwent one session of 3–4 pre-training trials in which they swam

in a rectangular channel (15 cm × 122 cm) and mounted a square platform (10 × 10 cm) hidden 1.5 cm below the water surface in the middle of the channel. If a mouse did not mount the platform within 10 s, it was guided to the platform by the experimenter and was allowed to sit on the platform for 10 s before being removed by the experimenter. The day after pre-training, the mice were trained in the circular water maze.

For hidden platform training, the platform was submerged 1.5 cm below the surface. The platform location remained the same throughout training, but the drop location varied randomly between the four daily trials. Mice received two sessions per day for 2–7 consecutive days, as indicated in the figures. Each session consisted of two trials with a 5–10-min inter-trial interval. The maximum time allowed per trial was 60 s. If a mouse did not find or mount the platform, it was guided to the platform by the experimenter. All mice were allowed to sit on the platform for 10 s after each training trial.

For probe trials, the platform was removed and each mouse was allowed to swim for 60 s. The drop location for the probe trials was 180° from the platform location used during hidden platform training. After 60 s, mice were guided to the platform location before retrieval from the pool. Young and aging *GFAP-Cre/loxP-Adora2a* mice probed on day 6 after training (Fig. 2b,h) were also probed on days 1 and 4 after training. On day 1 after training, *A_{2A}-cWT* mice showed minimal preference for the target quadrant and platform location, whereas *A_{2A}-cHET* and *A_{2A}-cKO* mice showed a significant preference for the target quadrant and platform location (data not shown). To improve the memory of *A_{2A}-cWT* mice and further test memory retention, two additional training trials were performed 2–3 h after the first probe. During the second probe on day 4 after initial training, all groups showed preference for the target quadrant and platform location (data not shown). For experiments involving two probe trials performed 1 h and 2 d after training (Fig. 6i–k), one additional training trial was performed immediately after the 1-h probe to reinforce the memory (data not shown). For experiments involving four probe trials (Fig. 6a–e), additional training was not performed after each probe in order to prevent mice from re-learning the platform location after each probe.

All behavior was recorded with a video tracking system (Noldus). Escape latencies, distance traveled, swim paths, swim speeds and platform crossings were recorded automatically for subsequent analysis.

Novel object-recognition test. Mice were acclimated to the testing room for 1 h and habituated to a square testing chamber (40 × 40 cm) for 15 min. During training, each mouse was presented with two identical objects in the same chamber and allowed to explore freely for 10 min once per day for two days. Two days after completion of training, each mouse was tested by being presented with one object used during training and one unfamiliar (novel) object of a different shape and texture. Which of the familiar objects was replaced with a novel object was varied randomly between mice to control for location bias. The objects used for training and testing were assigned randomly to each mouse to avoid object bias. Arenas and objects were cleaned with 70% ethanol after each mouse. Behavior was video-recorded and the frequency and duration of visits with each object were scored.

Open-field test. Spontaneous activity in the open field was measured using an automated Flex-Field/Open Field Photobeam Activity System (San Diego Instruments, San Diego, CA). After acclimation to the testing room for 1 h, mice were tested for 15 min in a clear plastic chamber (41 × 41 × 30 cm) with two 16 × 16 photobeam arrays detecting horizontal and vertical movements. For context-dependent habituation in the open field, chambers were surrounded by distinct proximal cues. Mice were habituated in 5-min trials (with a 3-h inter-trial interval) and tested in the same chambers at indicated times after habituation. In Figure 2e–f, mice were re-habituated to the open field for one day. Between then and re-testing in the same field on day 21, the mice were assessed in the Morris water maze as shown in Figure 2a–b. The apparatus was cleaned with 70% alcohol after each mouse. Total movements (i.e., ambulations), rearing in the open field, and time spent in the center and periphery of the open field were recorded automatically for subsequent analysis.

Elevated plus maze. The maze consisted of two open and two enclosed arms elevated 63 cm above the ground (Hamilton-Kinder, Poway, CA). After acclimation to the testing room for 1 h, mice were placed at the junction between the

open and closed arms of the maze and allowed to explore freely for 10 min. The maze was cleaned with 70% ethanol after each mouse. Total distance traveled and time spent in the open and closed arms were recorded automatically for subsequent analysis.

Y maze. The maze consisted of three symmetrical arms (spaced 120° apart) in the shape of a Y. After acclimation to the testing room for 1 h, mice were allowed to explore the maze freely for 6 min. The maze was cleaned with 70% alcohol after each mouse. Arm entries were recorded manually and spontaneous alternations (successive entries into each of the three arms) and total activity (number of arm entries) were calculated.

Rota-rod test. After acclimation to the testing room for 1 h, mice were placed on the Rota-Rod (Med Associates Inc.), which was rotated at a constant speed of 16 rpm. Photobeam interruptions caused by mice falling off the rotating rod were recorded. Photobeams were interrupted by the experimenter if the mouse held onto the rod without walking for three full rotations. Each mouse was given three trials with a 10-min inter-trial interval and a maximum of 300 s per trial. The average latency to fall off the Rota-Rod was calculated.

Hot-plate test. Nociceptive responses were tested using the surface of an aluminum hotplate heated to 52 °C. Mice were placed in a clear, open-ended cylindrical enclosure on top of the hotplate. The latency to respond with a hindpaw lick, hindpaw flick, or jump, whichever came first, was recorded manually. The maximum latency was set to 30 s, after which time the mice were removed from the hotplate.

Immunohistochemistry. Mice were anesthetized with Avertin (tribromoethanol, 250 mg per kg) and perfused transcardially with 0.9% saline for 1 min. Brains were removed, post-fixed in 4% paraformaldehyde (PFA) for 24 h, incubated in 30% sucrose for 1–3 days at 4 °C, and sectioned at a thickness of 30 µm using a freezing microtome (Leica SM 2000R). For *A_{2A}* receptor immunostaining shown in Figures 7 and 8 and Supplementary Figures 3a and 9–11, nonspecific binding was blocked with the blocking reagent provided in the mouse-on-mouse kit (Vector Laboratories). Sections were incubated overnight at room temperature in mouse monoclonal anti-*A_{2A}* receptor antibody (1:200, Millipore, 05-717)³ diluted in the diluent provided in the mouse-on-mouse kit. Donkey anti-mouse secondary antibodies conjugated to Alexa fluorophores (Life Technologies, 1:500, A21202 and A21203) were used to visualize primary antibody labeling. Photomicrographs were acquired using a Nikon TE300 microscope and Spot RT digital CCD camera and imaging software (Diagnostic Instruments). For *A_{2A}* receptor immunolabeling for confocal microscopy (Supplementary Fig. 3b,c), brains were sectioned with a vibratome and incubated overnight at 4 °C with a mouse monoclonal anti-*A_{2A}* receptor antibody (1:10,000, Millipore, 05-717)³ and a GFAP antibody (1:500, Millipore, MAB3402)⁶⁹ or NeuN antibody (1:1000, Millipore, MAB377)⁷⁰. *A_{2A}* receptor immunoreactivity was detected with the Tyramide Signal Amplification™-Direct (Red) system (1:100, NEN Life Sciences, Boston, MA), while GFAP and NeuN immunoreactivities were detected with a fluorescein-tagged secondary antibody (1:75, Vector Laboratories, Fl-2000)⁷¹. Control experiments were performed by incubating sections with non-immune IgG instead of primary antibodies and by single labeling and switching the tagged secondary antibodies. Sections were imaged with a Zeiss 63X (N.A. 1.4) objective on an Axiovert 35 microscope (Zeiss) with an attached MRC1024 laser scanning confocal microscope system (BioRad). Sections were analyzed with ImageJ to estimate the proportion of GFAP- or NeuN-positive cells displaying *A_{2A}* receptor immunoreactivity⁷².

For measurement of Arc levels, individual mice resting in their home cages during their daytime sleep cycle were rapidly anesthetized with Avertin and perfused with saline as described above. The right hemisphere of the brain was post-fixed in 4% PFA, incubated in sucrose and sectioned as described above, and the left hemisphere was frozen on dry ice for RNA assessment by qRT-PCR (described below). To block nonspecific binding, brain sections were incubated in 10% normal donkey serum, 1% nonfat dry milk, 0.2% gelatin and 0.5% Triton X-100 in PBS for 1 h at room temperature. Sections were incubated overnight at 4 °C in rabbit anti-Arc antibody (1:12,000, Synaptic Systems, 156-003)⁷³ diluted in 3% normal donkey serum, 0.2% gelatin, and 0.5% Triton X-100 in PBS. Biotinylated anti-rabbit secondary antibody (1:500, Jackson ImmunoResearch,

711-065-152) was diluted similarly to the primary antibody and applied to the sections for 1 h. An avidin-biotin complex kit (Vector Laboratories) and 3, 3'-diaminobenzidine tetrahydrochloride (Vector Laboratories) were used to visualize antibody labeling. Sections were imaged using a 10X objective (Nikon) and analyzed with a BZ-9000 automated microscope system and analysis application (Keyence). Arc immunoreactivity was quantified in the entire granular cell layer of the dentate gyrus in one rostral and one caudal section per mouse. To obtain high-resolution photomicrographs of the entire dentate gyrus within a brain section, multiple images were acquired and reconstructed automatically for each brain section. After cropping the images to isolate the dentate gyrus, thresholding was carried out using a constant value to eliminate background staining. Regions of interest representing individual cells were automatically visualized and quantified to obtain the total number of cells per section and the total area per section immunoreactive for Arc. These values were averaged per mouse and compared across genotypes.

For FLAG immunostaining, antigen retrieval was performed by incubating brain sections in citrate buffer (9.4 mM citric acid, 41 mM sodium citrate, adjusted to pH 6) at 100 °C for 45 min. Nonspecific binding was blocked with a mixture of 1% nonfat dry milk, 10% normal donkey serum, and the blocking reagent provided in the mouse-on-mouse kit (Vector Laboratories) diluted in PBST. Sections were incubated for 15 min in Avidin and Biotin blocking solutions (Vector Laboratories) before overnight incubation at 4 °C in mouse anti-FLAG M2 antibody (1:250, Sigma-Aldrich, F1804)⁵⁶ diluted in 3% normal donkey serum and the diluent provided in the mouse-on-mouse kit. Biotinylated anti-mouse secondary antibody (1:500, Jackson ImmunoResearch, 715-065-150) was diluted similarly to the primary antibody and applied to the sections for 1 h. Avidin-biotin complex kit (Vector Laboratories) and 3, 3'-diaminobenzidine tetrahydrochloride (Vector Laboratories) were used to visualize antibody labeling.

For co-immunolabeling studies, rabbit anti-glutamine synthetase antibody (1:600, Abcam, ab16802)⁷⁴ or rabbit anti-GFAP antibody (1:500, Sigma-Aldrich, G9269)^{75,76} was included with the anti-FLAG or anti-A_{2A} receptor antibodies. Donkey anti-rabbit and donkey anti-mouse antibodies conjugated to Alexa fluorophores (1:500, Life Technologies, A21202, A21203, A21206, and A20207) were used to visualize primary antibody labeling. Sections were analyzed with ImageJ to count the number of GFAP-positive cells expressing FLAG in the hippocampus of GFAP-Rs1 mice and to measure the mean intensity of A_{2A} immunolabeling in the hilus of triply transgenic mice. For pERK immunostaining, nonspecific binding was blocked with 10% normal donkey serum and 0.5% Triton X-100 in Tris-buffered saline for 1 h and incubated overnight at 37 °C in rabbit anti-phospho-ERK1/2 antibody (T202/Y204, 1:200, Cell Signaling, 9101)⁷⁷.

For Thioflavin-S staining of amyloid plaques, brain sections were incubated for 5 min in a solution containing 0.005% Thioflavin-S (Sigma-Aldrich, T1892) and 75% ethanol in PBS. Amyloid plaques were also detected by blocking nonspecific binding with 10% normal donkey serum and 0.5% Triton X-100 in Tris-buffered saline for 1 h and overnight incubation at 4 °C in mouse anti-A_B antibody 6E10 (1:500, Covance, SIG-39320)⁷⁸. Donkey anti-mouse antibody conjugated to Alexa-488 (1:500, Life Technologies, A21202) was used to visualize primary antibody labeling.

Protein extraction. Mice were anesthetized with Avertin (tribromoethanol, 250 mg per kg) and perfused transcardially with 0.9% saline. Brains were removed, microdissected in ice-cold PBS, and homogenized in ice-cold buffer containing 1X PBS (pH 7.4), 1 mM 1,4-Dithiothreitol (DTT, Roche), 0.5 mM EDTA, 0.5% Triton X-100, 0.1 M phenylmethyl sulfonyl fluoride (PMSF), a protease inhibitor cocktail (Roche), and phosphatase inhibitor cocktail (Sigma-Aldrich). Homogenates were sonicated twice for 5 min at 40 Amp and centrifuged at 10,000 rpm for 10 min at 4 °C. The supernatants were collected for measurement of protein concentrations and western blotting.

Astrocyte cultures were lysed on ice for 10 min using a lysis buffer containing 10 mM Tris (pH 7.4), 150 mM NaCl, 0.5% deoxycholate, 5 mM EDTA, 0.2% Triton X-100, a protease inhibitor cocktail (Roche) and a phosphatase inhibitor cocktail (Sigma-Aldrich). The lysates were sonicated for 1 min at 40 Amp and centrifuged at 10,000 rpm for 10 min at 4 °C. The supernatants were collected for measurement of protein concentrations and western blotting.

Western blotting. Proteins (10–20 µg/well) were separated using a 4–12% NuPAGE Bis-Tris gel (Life Technologies) and transferred onto nitrocellulose

membranes, which were incubated for 1 h in 5% bovine serum albumin (Sigma-Aldrich) diluted in Tris-buffered saline containing 0.05% Tween (BSA-TBST). Membranes were incubated overnight at 4 °C in rabbit anti-phospho-CREB (S133, 1:1,000, Cell Signaling, 9198)⁷⁹ or rabbit anti-phospho-ERK1/2 (T202/Y204, 1:2,000, Cell Signaling, 9101)⁷⁷ antibodies diluted in BSA-TBST. Bound antibodies were detected using horseradish peroxidase-conjugated goat anti-rabbit antibody (1:3,000, Calbiochem, 401393) diluted in BSA-TBST. Chemiluminescent bands were visualized using an ECL system (Pierce) and quantified densitometrically.

Levels of total CREB and ERK1/2 protein were detected after stripping the membranes for 1 h at 55 °C with a buffer containing 10% SDS, 1 M Tris (pH 6.7), and 0.7% β-mercaptoethanol. Stripped membranes were incubated for 1 h in BSA-TBST and overnight at 4 °C in mouse anti-CREB (1:1,000, Millipore, MAB5432)⁸⁰ or rabbit anti-ERK1/2 (1:4,000, Cell Signaling, 4696)⁸¹ antibody diluted in BSA-TBST. Rabbit anti-GFAP antibody (1:3,000, Sigma-Aldrich, G9269)^{75,76} and mouse monoclonal anti-A_{2A} receptor antibody (1:500, Millipore, 05-717)³ were diluted in TBST containing 5% nonfat dry milk (milk-TBST). Bound antibodies were detected as described above.

Immunoprecipitation. FLAG-Rs1 protein expression in cultured astrocytes was detected using the Pierce Crosslink Immunoprecipitation kit with minor modifications to the manufacturer's instructions (Thermo Scientific). Briefly, 5 µg of 5HT₄ receptor antibody (R&D Systems, MAB6545) were cross-linked to 20 µl of Pierce Protein A/G Plus Agarose beads. Astrocyte cultures were lysed as detailed above and the lysates (150 µg of protein) were pre-cleared with 15 µl of Control Agarose Resin slurry (Thermo Scientific) for 1 h at 4 °C. The pre-cleared lysates were incubated with antibody-bound beads overnight at 4 °C. The bound protein was eluted with 30 µl elution buffer and mixed with 10 µl of 4X sample buffer (Life Technologies) and 5 µl of 10X reducing agent (Life Technologies). After incubating the mixture at 70 °C for 10 min, the proteins were separated on a 4–12% NuPAGE Bis-Tris gel and transferred onto nitrocellulose membranes. The membranes were incubated for 1 h in milk-TBST and overnight at 4 °C in rabbit anti-FLAG antibody (1:1,000, Abcam, 21536)⁸² diluted in milk-TBST. Bound antibodies were detected and visualized as described above.

qRT-PCR. Total RNA was isolated from microdissected frozen mouse brain tissue with the RNeasy Mini kit (Qiagen) and reverse transcribed with random hexamers and oligo(dT) primers. The TaqMan gene expression assay and ABI Prism 7900 sequence detector (Applied Biosystems) were used to determine the levels of Rs1 (based on the human HTR4B) and β-actin (mouse Actb) mRNA. The following ABI probes were used: Hs00168380_m1-FAM for detection of human HTR4B mRNA, Mm00607939_s1-VIC for detection of mouse Actb mRNA, Mm00479619_g1-FAM for detection of mouse Arc mRNA, and Mm99999915_g1-VIC for detection of mouse Gapdh mRNA. Human HTR4B mRNA was not detected in brain tissue from GFAP-tTA singly transgenic mice (data not shown). For quantification, HTR4B/Actb ratios were normalized to the average ratios in young GFAP-Rs1 mice, and Arc/Gapdh ratios were normalized to the average ratios in control mice.

Levels of Gfap and Gapdh mRNA in GFAP-Rs1 mice were determined using SYBR green PCR reagents and the ABI Prism 7700 sequence detector according to the manufacturer's instructions (Applied Biosystems). The following primer sequences were used: Gfap forward: GGAGTGGTATCG GTCTAAGTTGC; Gfap reverse: GCGATAGTCGTTAGCTCGTGT; Gapdh forward: GGGAAAGCCCATCACCATCTT; Gapdh reverse: GCCTTCTCCATGGTGGTGAA.

For quantification, Gfap/Gapdh ratios were normalized to the average ratios in young GFAP-tTA mice. The quality of all primers and amplification reactions was assessed by analysis of dissociation curves, standard curve slopes and reactions lacking reverse transcriptase.

cAMP measurements. Intracellular cAMP levels in primary astrocyte cultures were measured by CatchPoint Cyclic-AMP Fluorescence Assay (Molecular Devices) with minor modifications to the manufacturer's instructions. Primary astrocytes from postnatal day 1–3 mouse pups were plated with supplemented DMEM in 96-well plates coated with poly-D-lysine (50 µg/ml). After 4–5 days in culture, cells were washed with fresh medium and some wells were transduced with Lenti-Rs1, Lenti-A_{2A}, or Lenti-mCherry. After 5–10 days, cells were treated with 0.75 mM 3-isobutyl-1-methylxanthine (Sigma-Aldrich) diluted in

HBSS containing 10 mM glucose for 10 min to inhibit phosphodiesterase activity. Agonists were diluted in HBSS and applied onto cells for 15 min at 37 °C. Following cell lysis, the lysates were transferred onto anti-rabbit IgG-coated 96-well plates. Some wells received unconjugated cAMP instead of lysate to obtain a calibration curve for each assay plate and trial. All samples were incubated with anti-cAMP antibody and horseradish peroxidase-conjugated cAMP for 2 h. Following development with Stoplight Red substrate, fluorescence intensity within each well was measured at 530-nm excitation and 590-nm emission using the FlexStation II plate reader (Molecular Devices).

Calcium measurements. Intracellular calcium levels in primary astrocyte cultures were measured by Fluorometric Imaging Plate Reader (FLIPR) Calcium-5 Assay (Molecular Devices) with minor modifications to the manufacturer's instructions. Primary astrocytes from postnatal day 1–3 mouse pups were plated with supplemented DMEM in 96-well plates coated with poly-D-lysine (50 µg/ml). After 4–5 days in culture, cells were washed with fresh medium and some wells were transduced with Lenti-Rs1, Lenti-A_{2A}, or Lenti-mCherry. After 5–10 days, cells were incubated in Calcium-5 dye dissolved in HBSS containing 20 mM HEPES for 1 h at 37 °C. Fluorescence intensity 30 s before and 2 min after agonist or vehicle (HBSS) application within each well was measured every 2 s at 485-nm excitation and 525-nm emission using the FlexStation II plate reader (Molecular Devices).

Human brain tissues. For immunohistochemistry, post-mortem human brain tissue blocks or sections from control and AD cases were obtained from the New York Brain Bank at Columbia University Medical Center, Banner Sun Health Research Institute (Sun City, Arizona), and the Alzheimer's Disease Research Center at the University of California, San Diego (Supplementary Table 1). Formalin-fixed tissue blocks were incubated in 30% sucrose for 3–5 days at 4 °C and sectioned at a thickness of 50 µm using a freezing microtome (Leica SM 2000R). Antigen retrieval was performed by incubating brain sections in citrate buffer (pH 6) at 100–115 °C for 15 min. Nonspecific binding was blocked by incubation for 2 h in the blocking reagent provided in the mouse-on-mouse kit (Vector Laboratories). Sections were incubated for 15 min in Avidin and Biotin blocking solutions (Vector Laboratories) before overnight incubation at room temperature in mouse anti-A_{2A} receptor antibody (1:50, Millipore, 05-717)³ diluted in the diluent provided in the mouse-on-mouse kit. Biotinylated anti-mouse secondary antibody (1:250, Jackson ImmunoResearch, 715-065-150) was diluted similarly to the primary antibody and applied to the sections for 1 h. Avidin-biotin complex kit (Vector Laboratories) and 3,3'-diaminobenzidine tetrahydrochloride (Vector Laboratories) were used to visualize antibody labeling. For co-immunolabeling, the sections were incubated in 0.3% Sudan Black B (Sigma-Aldrich) in 70% ethanol for 20 min after antigen retrieval to reduce tissue autofluorescence. Mouse anti-A_{2A} receptor antibody (1:50, IgG2a, Millipore, 05-717)³ was co-applied with mouse anti-Aldh1L1 antibody (1:300, IgG1, NeuroMab, clone N103-39, 75-140)⁸³ or goat anti-Iba1 antibody (1:200, Abcam, ab5076)⁸⁴. Anti-mouse IgG2a (1:250, Life Technologies, A21131) anti-mouse IgG1 (1:250, Life Technologies, A21125), or anti-goat IgG antibodies (1:500, Life Technologies, A11058) conjugated to Alexa fluorophores were used to visualize primary antibody labeling. Photomicrographs were acquired with a Nikon TE300 microscope and Spot RT digital CCD camera and imaging software (Diagnostic Instruments).

For western blotting, post-mortem human brain tissue blocks from control and AD cases were obtained from the New York Brain Bank at Columbia University Medical Center, the Alzheimer's Disease Research Center at the University of California, San Diego, and the Memory and Aging Center at the University of California, San Francisco (see Supplementary Table 1). Hippocampi and frontal cortices were microdissected from tissue blocks in ice-cold PBS and homogenized in RIPA buffer. Proteins (10–20 µg/well) were separated on a 4–12% NuPAGE Bis-Tris gel (Life Technologies) and transferred onto nitrocellulose membranes, which were incubated for 1 h in milk-TBST. Membranes were incubated overnight at 4 °C in mouse anti-A_{2A} receptor antibody (1:500, Millipore, 05-717)³. Bound antibodies were detected using horseradish peroxidase-conjugated goat anti-mouse antibody (1:3,000, Calbiochem, 401253). Chemiluminescent bands were visualized with an ECL system (Pierce) and quantified densitometrically. For detecting actin, membranes were stripped and incubated for 1 h in

milk-TBST and overnight at 4 °C in rabbit anti-actin antibody (1:5,000, Sigma-Aldrich, A2066)⁸⁵ diluted in milk-TBST.

For qRT-PCR, post-mortem human brain tissue blocks from control and AD cases were obtained from the New York Brain Bank at Columbia University Medical Center (see Supplementary Table 1). The dentate gyrus was dissected from frozen brain tissue blocks. Total RNA was isolated using the RNeasy Mini kit (Qiagen) and reverse transcribed with random hexamers and oligo(dT) primers. Brain pH, RNA quality and postmortem intervals did not differ between the groups (data not shown). The following primer sequences were used: GAPDH forward: CCCATGTTCTCATGGGT; GAPDH reverse: TGGTCATGAGTCCTCCACGATA; GFAP forward: TGGAGCTCAATGACCGCTT; GFAP reverse: GCGCCTGTTTGCTGTT; ADORA2A forward: CCGTATCCGCGAGTCCGCC; ADORA2A reverse: GCACTGGTGCCAGCTGCCTT.

Statistical analyses. Data are presented as mean ± s.e.m. All statistical tests were performed with GraphPad Prism (version 5). Sample sizes were determined by pilot experiments and previous studies with similar types of experiments. Normality was tested by D'Agostino and Pearson omnibus normality test. The criterion for data point exclusion was established during the design of the study and was set to values above or below two s.d. from the group mean. Variances between two groups were compared by F test and differences between two groups by unpaired Student's *t* test (two-tailed, unless indicated otherwise in the figure legends). Welch's correction was used to account for unequal variances between two groups. Quadrant preference in the Morris water maze was assessed by two-tailed one-sample *t* test and FDR correction for multiple comparisons. Differences among multiple groups were assessed by one-way or two-way ANOVA followed by Dunnett's or Bonferroni multiple comparisons post-hoc tests, as specified in the figure legends. Correlations were assessed by linear regression and Spearman's correlation. Null hypotheses were rejected at *P* < 0.05.

A **Supplementary Methods Checklist** is available.

51. Chen, J.F. *et al.* A(2A) adenosine receptor deficiency attenuates brain injury induced by transient focal ischemia in mice. *J. Neurosci.* **19**, 9192–9200 (1999).
52. Lin, W. *et al.* Interferon-gamma induced medulloblastoma in the developing cerebellum. *J. Neurosci.* **24**, 10074–10083 (2004).
53. Conklin, B.R. *et al.* Engineering GPCR signaling pathways with RASSLs. *Nat. Methods* **5**, 673–678 (2008).
54. Hsiao, E.C. *et al.* Osteoblast expression of an engineered Gs-coupled receptor dramatically increases bone mass. *Proc. Natl. Acad. Sci. USA* **105**, 1209–1214 (2008).
55. Halassa, M.M. *et al.* Astrocytic modulation of sleep homeostasis and cognitive consequences of sleep loss. *Neuron* **61**, 213–219 (2009).
56. Sweger, E.J., Casper, K.B., Scearce-Levie, K., Conklin, B.R. & McCarthy, K.D. Development of hydrocephalus in mice expressing the G(i)-coupled GPCR Ro1 RASSL receptor in astrocytes. *J. Neurosci.* **27**, 2309–2317 (2007).
57. Pascual, O. *et al.* Astrocytic purinergic signaling coordinates synaptic networks. *Science* **310**, 113–116 (2005).
58. Kawamata, H. *et al.* Abnormal intracellular calcium signaling and SNARE-dependent exocytosis contributes to SOD1G93A astrocyte-mediated toxicity in amyotrophic lateral sclerosis. *J. Neurosci.* **34**, 2331–2348 (2014).
59. Fujita, T. *et al.* Neuronal transgene expression in dominant-negative SNARE mice. *J. Neurosci.* **34**, 16594–16604 (2014).
60. Sloan, S.A. & Barres, B.A. Looks can be deceiving: Reconsidering the evidence for gliotransmission. *Neuron* **84**, 1112–1115 (2014).
61. Rockenstein, E.M. *et al.* Levels and alternative splicing of amyloid beta protein precursor (APP) transcripts in brains of APP transgenic mice and humans with Alzheimer's disease. *J. Biol. Chem.* **270**, 28257–28267 (1995).
62. Palop, J.J. *et al.* Aberrant excitatory neuronal activity and compensatory remodeling of inhibitory hippocampal circuits in mouse models of Alzheimer's disease. *Neuron* **55**, 697–711 (2007).
63. Sullivan, P.M., Mace, B.E., Maeda, N. & Schmechel, D.E. Marked regional differences of brain human apolipoprotein E expression in targeted replacement mice. *Neuroscience* **124**, 725–733 (2004).
64. Raber, J. *et al.* Isoform-specific effects of human apolipoprotein E on brain function revealed in *ApoE* knockout mice: Increased susceptibility of females. *Proc. Natl. Acad. Sci. USA* **95**, 10914–10919 (1998).
65. Leung, L. *et al.* Apolipoprotein E4 causes age- and sex-dependent impairments of hilar GABAergic interneurons and learning and memory deficits in mice. *PLoS ONE* **7**, e53569 (2012).
66. Colin, A. *et al.* Engineered lentiviral vector targeting astrocytes *in vivo*. *Glia* **57**, 667–679 (2009).
67. Shigetomi, E., Kracun, S. & Khakh, B.S. Monitoring astrocyte calcium microdomains with improved membrane targeted GCaMP reporters. *Neuron Glia Biol.* **6**, 183–191 (2010).

68. Zlatkine, P., Mehl, B. & Magee, A.I. Retargeting of cytosolic proteins to the plasma membrane by the Lck protein tyrosine kinase dual acylation motif. *J. Cell Sci.* **110**, 673–679 (1997).
69. Hagemann, T.L., Jobe, E.M. & Messing, A. Genetic ablation of Nrf2/antioxidant response pathway in Alexander disease mice reduces hippocampal gliosis but does not impact survival. *PLoS ONE* **7**, e37304 (2012).
70. Saaltink, D.J., Havik, B., Verissimo, C.S., Lucassen, P.J. & Vreugdenhil, E. Doublecortin and doublecortin-like are expressed in overlapping and non-overlapping neuronal cell population: Implications for neurogenesis. *J. Comp. Neurol.* **520**, 2805–2823 (2012).
71. Spencer, B. *et al.* Beclin 1 gene transfer activates autophagy and ameliorates the neurodegenerative pathology in alpha-synuclein models of Parkinson's and Lewy body diseases. *J. Neurosci.* **29**, 13578–13588 (2009).
72. Marxreiter, F. *et al.* Glial A30P alpha-synuclein pathology segregates neurogenesis from anxiety-related behavior in conditional transgenic mice. *Neurobiol. Dis.* **59**, 38–51 (2013).
73. Piatti, V.C. *et al.* The timing for neuronal maturation in the adult hippocampus is modulated by local network activity. *J. Neurosci.* **31**, 7715–7728 (2011).
74. Mangin, J.M., Li, P., Scafidi, J. & Gallo, V. Experience-dependent regulation of NG2 progenitors in the developing barrel cortex. *Nat. Neurosci.* **15**, 1192–1194 (2012).
75. Olabarria, M., Noristani, H.N., Verkhratsky, A. & Rodriguez, J.J. Concomitant astrogliat atrophy and astrogliosis in a triple transgenic animal model of Alzheimer's disease. *Glia* **58**, 831–838 (2010).
76. Nicole, O. *et al.* Activation of protease-activated receptor-1 triggers astrogliosis after brain injury. *J. Neurosci.* **25**, 4319–4329 (2005).
77. Moritz, A. *et al.* Akt-RSK-S6 kinase signaling networks activated by oncogenic receptor tyrosine kinases. *Sci. Signal.* **3**, ra64 (2010).
78. Terai, K. *et al.* beta-amyloid deposits in transgenic mice expressing human beta-amyloid precursor protein have the same characteristics as those in Alzheimer's disease. *Neuroscience* **104**, 299–310 (2001).
79. Kir, S. *et al.* Tumour-derived PTH-related protein triggers adipose tissue browning and cancer cachexia. *Nature* **513**, 100–104 (2014).
80. Yiu, A.P., Rashid, A.J. & Josselyn, S.A. Increasing CREB function in the CA1 region of dorsal hippocampus rescues the spatial memory deficits in a mouse model of Alzheimer's disease. *Neuropsychopharmacology* **36**, 2169–2186 (2011).
81. Syme, C.A., Friedman, P.A. & Bisello, A. Parathyroid hormone receptor trafficking contributes to the activation of extracellular signal-regulated kinases but is not required for regulation of cAMP signaling. *J. Biol. Chem.* **280**, 11281–11288 (2005).
82. Sivachandran, N., Sarkari, F. & Frappier, L. Epstein-Barr nuclear antigen 1 contributes to nasopharyngeal carcinoma through disruption of PML nuclear bodies. *PLoS Pathog.* **4**, e1000170 (2008).
83. Yang, Y. *et al.* Molecular comparison of GLT1⁺ and ALDH1L1⁺ astrocytes *in vivo* in astrogli reporter mice. *Glia* **59**, 200–207 (2011).
84. Coppieters, N. *et al.* Global changes in DNA methylation and hydroxymethylation in Alzheimer's disease human brain. *Neurobiol. Aging* **35**, 1334–1344 (2014).
85. Kocherhans, S. *et al.* Reduced Reelin expression accelerates amyloid-beta plaque formation and tau pathology in transgenic Alzheimer's disease mice. *J. Neurosci.* **30**, 9228–9240 (2010).